

## Topical Review

# A review of interferometry for geometric measurement

Shuming Yang<sup>ID</sup> and Guofeng Zhang

State Key Laboratory for Manufacturing Systems Engineering, Xi'an Jiaotong University, Xi'an, Shaanxi 710049, People's Republic of China

E-mail: [shuming.yang@mail.xjtu.edu.cn](mailto:shuming.yang@mail.xjtu.edu.cn)

Received 24 February 2018, revised 25 July 2018

Accepted for publication 31 July 2018

Published 4 September 2018



### Abstract

As high-precision measuring instruments have developed, interferometers have been widely applied in the measurement of lengths and of the shape of surfaces, with nanometer precision. The emergence of the laser is one of the revolutions that has led to a well-defined traceability route to the definition of the meter via interferometry. Another change is the ever-increasing adoption of detector arrays substituting for conventional methods of recording and analyzing interferograms. New applications have also arisen from the adoption of microscopes, optical fibers, chip-level components and diffractive optical elements, developing enhanced analogues of conventional interferometers, which have the advantages of high integration, low noise levels, and complete sets of measuring instruments with a high level of automation. Since the requirements for measurement parameters and the environment are becoming more complex, we expect that the related instruments will play a progressively significant role in the progress of advanced manufacturing processes and quality control. Multi-sensor integrated flexible measurement methods have been proposed to perform measurements with holistic, more accurate and reliable information. However, most of the proposed methods are not intelligent and are highly integrated, providing only specific solutions for given measuring tasks. In this paper, the principles, progress, prospects and development trends of interferometry are reviewed.

Keywords: interferometry, multi-sensor integration, flexible measurement

(Some figures may appear in colour only in the online journal)

### 1. Introduction

Dimension measurement and surface metrology of nano- and microstructures are increasingly in demand following rapid developments in many branches of science and industry such as semiconductors, precision engineering, microelectromechanical systems (MEMS) and materials science. The size of these structures ranges from nanometers to hundreds of micrometers. To fulfil these demands, advanced metrology techniques using contact and noncontact (optical) methods have been adopted for dimension measurement and surface metrology [1, 2]. Contact methods such as stylus profilers and

scanning probe microscopy (SPM) perform measurements point-wise with probes physically contacting the object surface; the measurement process is time-consuming and damages the testing surface. Both SPMs and stylus instruments have a limited lateral resolution caused by the interaction of the probe tip in contact with the peaks and valleys of the surface. In particular, SPMs have near-atomic spatial resolution for the measurement of smooth surfaces. However, for chopping surfaces with slopes of a few degrees or more, they seem to lose this superiority because the many points on the tip interact with surfaces simultaneously [3]. Optical methods have the advantage that they are noncontact, and they also

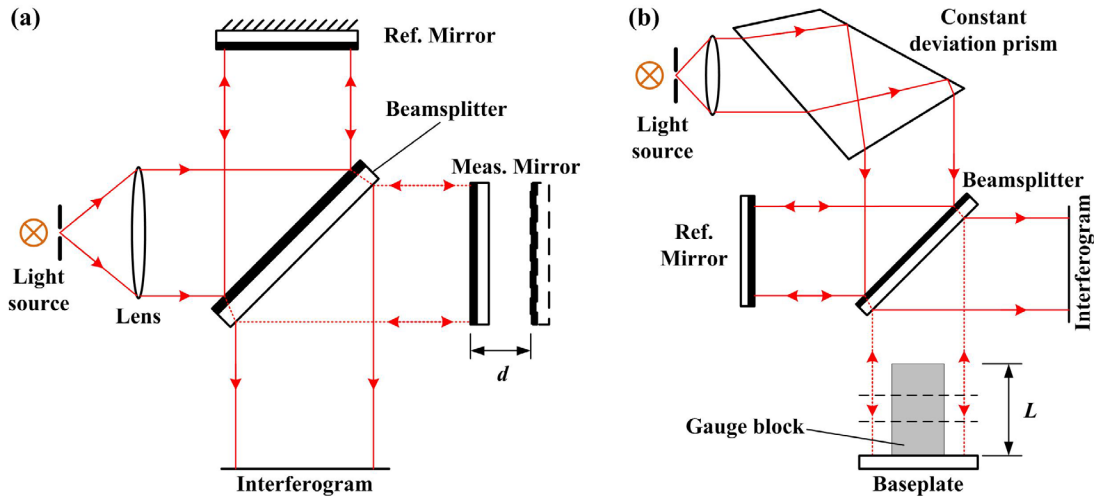


**Figure 1.** Michelson/Twyman–Green configuration. (a) Length/surface interferometry. (b) Gauge block interferometry; the constant deviation prism is a turning element which can invariably transform the propagating direction of the light beam.

have a faster measurement speed than contact methods using visual sensors. For these reasons, light is an indispensable tool for dimensional and surface metrology, and various optical methods have been proposed such as the laser triangulation method [4, 5], the optical lever method [6], the structured light method [7, 8], confocal microscopy [9, 10] and optical interferometry [11, 12].

For any measurement to be meaningful it needs to be traceable to its fundamental unit of measurement; in the case of length and surface measurement, this unit is the meter, which was defined as the length of the path travelled by light in a vacuum during the time interval of 1/299 792 458 of a second, and is practically realized via interferometry using the wavelength of an iodine-stabilized laser [13, 14]. Interferometry has therefore been widely applied because of the natural superiority of traceability, as well as its large dynamic measuring range, high sensitivity and resolution [15]. Since the Michelson interferometer was invented in 1881, various types of interferometry methods have been developed for displacement, distance, profile and surface measurement. Optical interferometry could be categorized by a variety of criteria: on the one hand, it can be classified according to the types of interference configurations, such as Michelson, Fizeau, Linnik, Mirau, Twyman–Green, Mach–Zehnder and Fabry–Perot interferometers [16]. Or it can be classified by the light source or the number of wavelengths used in the apparatuses, such as single wavelength interferometry, multi-wavelength interferometry (MWI) and white light interferometry (WLI) [17], which have different measuring ranges for use in different measurement tasks. Other enhanced applications have also arisen responding to specific requirements, such as digital holography, speckle and shearing interferometry [18, 19], as well as fiber optic interferometry [20], and diffractive interferometry [21]. Each measurement method has advantages and limitations regarding measurement resolution, range and application.

This paper provides an overview of interferometry methods used in length measurement and surface metrology, considering present difficulties and limitations in measurement for

each method. Multisensor integrated measurement systems ensuring high metrological standards, for measurement of an area of significant interest, are summarized and discussed in terms of recently presented proposals and solutions.

## 2. Traceability and uncertainty in interferometric measurements

### 2.1. General considerations in interferometry

Traceability is the property of a measurement result by which the result can be traced to a known standard through an unbroken chain of comparisons, each contributing to the measurement uncertainty [22]. Michelson and Benoit [23] were the pioneers who developed an interferometer to measure the length of the international prototype meter in terms of the wavelength, by which the definition of the meter was realized after the invention of lasers in the 1960s. If the wavelength is used as the reference, the primary length standards are generally iodine stabilized lasers that generate a stable frequency from a Fabry–Perot cavity [24, 25]. Surface characterization can be regarded as a set of height values of points covering an interferogram where a charge-coupled device (CCD) is adopted and the phase difference among points on the object maps the surface features. Gauge blocks [26], as material standards of length that need to be calibrated for conformity within an interferometer by using wavelength standards, are also widely adopted to provide industry with traceable and reliable standards of length.

The schematics of interferometers discussed in this chapter, considering the measurement traceability and uncertainty, are illustrated in figure 1. The typical Michelson configuration is adopted in length and gauge block interferometry. The Twyman–Green interferometer is a variant of the Michelson interferometer generally used for surface interferometry. The displacement  $z$  (distance or surface deviation) in the direction of the optical axis can be given by

$$z(x, y) = \frac{\lambda_\nu}{2n} \left( N + \frac{\varphi_m(x, y) - \varphi_r(x, y)}{2\pi} \right), \quad (1)$$

where  $x, y$  are the coordinates of the measuring and reference surfaces normal to  $z$ ;  $\varphi_m$  and  $\varphi_r$  are the phases at the measuring and reference surfaces, respectively;  $\lambda_v$  refers to the vacuum wavelength,  $n$  the air refractive index and  $N$  the integer number of  $\lambda_v/2n$ .

The displacement can be measured by counting the integer number and calculating the fraction, namely phase difference  $\Delta\phi = \varphi_m - \varphi_r$ . The measuring range depends on the coherence length of the source adopted and can be of one to tens of meters for commercial laser interferometers. Although subnanometer resolution can be realized in the vertical direction, interferometry methods may fail to meet the requirements of subnanometer resolution in the lateral directions because of the diffraction limit, i.e. the lateral resolution  $d$  is limited by

$$d \approx \frac{\lambda}{2 \cdot NA}, \quad (2)$$

where  $NA$  refers to the numerical aperture of the objective. By calculating, for example, in the visible light range, full-field microscopic interferometers are only available for micrometrology, finding it difficult to deal with measurements where nano-level lateral resolution is required.

## 2.2. Traceability and nonlinearity in length interferometry

The displacement measuring interferometer (DMI) uses the classical Michelson setup, and is applied in a range of occasions where subnanometer uncertainties are needed, especially the calibration of 1D scale [27]. For traceability to international standards, DMIs can present a direct link to primary length standards [28]. To link laser frequencies with the time standard, optical frequency combs have been exploited to perform the most accurate frequency comparisons of laser frequency standards using femtosecond lasers [29].

Equation (1) points out the direct error sources— $\lambda$ ,  $N$  and  $\Delta\phi$ . They arise from the nonstabilized laser source, misaligned optics, mechanical vibration, temperature and air disturbance. If all these conditions can be well controlled, the practical restrictions will be introduced by the nonlinearity. DMIs can operate with single-frequency (homodyne) or dual-frequency (heterodyne). The nonlinearity that determines the fraction of a wavelength was first reported by Quenelle [30] in heterodyne interferometers in 1983, and then experimentally observed by Sutton [31]. It is also called periodic error because it periodically repeats for each value of  $N$  with the same  $\Delta\phi$ . The nonlinearity in both heterodyne and homodyne interferometers was theoretically analyzed by Wu and Su [32], and generally varies from subnanometer level to several nanometers. This study found that the homodyne interferometer only has a second-order nonlinearity while the heterodyne interferometer has both its first- and second-order, which arise from the crosstalk between frequencies of two linearly polarized beams; the first-order nonlinearity can be compensated online, but the second-order nonlinearity is impossible to eliminate. Ellis *et al* [33] discussed the general error model and compensation strategy, and extensive research carried out into modeling and correcting these errors was reported in [34].

Some approaches for calibrating the phase difference have been exploited, including sharpening the interferogram using a Fabry–Perot interferometer (FPI) and using either a capacitive transducer or a frequency shifter [35]. A new alternative was presented by x-ray interferometry (XRI), where the effective wavelength is limited to 0.192 nm (the crystal lattice spacing [36]) and thus picometer resolution is achievable. The range of a monolithic XRI is limited to a few micrometers, so it is often combined with laser interferometry [37].

## 2.3. Traceability in surface interferometry

Surface interferometry can be performed using the Twyman–Green setup, but in the Fizeau configuration, in which the aberrations of the imaging system are common path [38] and thereby considered self-compensated. The uncertainty in the wavelength seems unimportant to traceability. The phase calibration is of the essence to traceability and the measured surface is usually characterized relative to a standard surface which is used as the reference and should be calibrated with reversal techniques [39]. Schulz *et al* [40] analyzed the traceability route and evaluated the related uncertainties for surface interferometry. They showed that for flatness measurement the calibration of the reference surface has the major contribution in the traceability chain; for sphericity measurement it is the same as flatness measurement, but the radius measurement is difficult; for aspheric measurement the traceability is particularly complicated and can generally only be resolved by virtual modeling of the experiments.

In surface interferometry the difference of  $N$  may vary over the surface measured in the case of flatness errors or mirror tilt, and then its determination becomes crucial. It is easy to determine for noise-free measurements on smooth surfaces, but it became annoying in the presence of noise or in measuring rough surfaces, in which we could not tell a real phase jump from the noise [41]. To determine the field number a great number of approaches and mathematical complications were reported in [42].

Compared to DMI, the vertical measuring range of microscopic interferometers is also limited by the focal depth of the objective. The measuring range is further decreased when the WLI is applied to perform unambiguous measurement with subnanometer vertical resolution. In WLI, the measured surface moves along the beam propagation direction and a full-field surface topography can be drawn by recording the coherence peak positions for all pixels imaged on the CCD. The wavelength bandwidth controls the resolution, and the traceability is derived by the positioning mechanism. Next to confocal microscopy [43], the WLI microscope is now the most commonly applied technology in surface characterization.

## 2.4. Calibration of gauge blocks by interferometry

The interferometric calibration of a gauge block (GB) ensures traceability from the optical realization of meter to material standards. The length of a GB is defined as the perpendicular distance between a selected point of the GB surface and the

platen [44] to which the gauge is wrung, as shown in figure 2. The measurement system setup is based on the Twyman–Green interferometer (figure 1(b)), from which we can see this definition is selected such that the optical and mechanical lengths are equal, i.e. the plane wave of the interferometer has the same phase on reflection from the GB and the platen, for one-sided probing and to cancel any wringing effect when multiple GBs are wrung together [40].

To calibrate the gauge block, a series of fringe fractions  $f_1, \dots, f_n$  is obtained at the standard wavelengths  $\lambda_i$ . Usually an adjustable constant deviation prism is adopted to choose a single wavelength to illuminate the interferometer. The optical length  $L$  is then calculated by

$$L = (M_1 + f_1) \frac{\lambda_1}{2} = (M_2 + f_2) \frac{\lambda_2}{2} = \dots = (M_n + f_n) \frac{\lambda_n}{2}, \quad (3)$$

where  $M_i$  refers to the interference order of each wavelength. A number of calibrations are needed to convert the optical path to the GB length. Interferometry can calibrate this material length with an uncertainty of from 30 to 70 nm [45]. The surface of the GB must be evaluated to ensure that the nonflatness, parallelism, and length variation of each measuring surface is within the tolerances set for the particular grade of GB under calibration [46]. Modern instruments have incorporated phase-stepping interferometry to assess the GBs [46–48].

The requirement on the stability and accuracy of the wavelength in gauge block interferometry (GBI) is even greater than in DMI [49]. In GBI a small deviation in the frequency can result in excessive errors when it is used for the calibration of larger lengths of more than 1 m, e.g. an error of  $4 \times 10^{-8}$  will lead to the wrong calculated  $N$  with the error of  $3 \times 10^{-7}$  (a fringe in 1 m). Therefore, the maximum measurable length will be limited if the frequency of the source is not stable. The base platen flatness and the reference mirror flatness are of equal importance in GBI. Additional sources of uncertainty are the aperture correction for collimated beams from a finite source and the wringing correction for the case that the platen and GB are not of the same material or surface roughness [40]. A new GBI system which does not need wringing onto a base platen has been developed by Kuriyama *et al* [50]. It is difficult to obtain uncertainties at the nano-level ( $< 10$  nm) using GBI since its components have the most errors.

### 3. Interferometric techniques for length measurement

#### 3.1. Displacement measurement

**3.1.1. Homodyne versus heterodyne detection.** The simplest interferometer can be considered as a homodyne or polarization interferometer, based on the measurement of intensity variation at the detector [51]. A robust commercial implementation can be seen in figure 3, and it generally includes three parts: the stabilized single frequency laser source, the interferometer part, and the detection and signal processing part. In the laser source part (figure 3(a)), the wavelength is determined by the laser tube length which is changed by varying

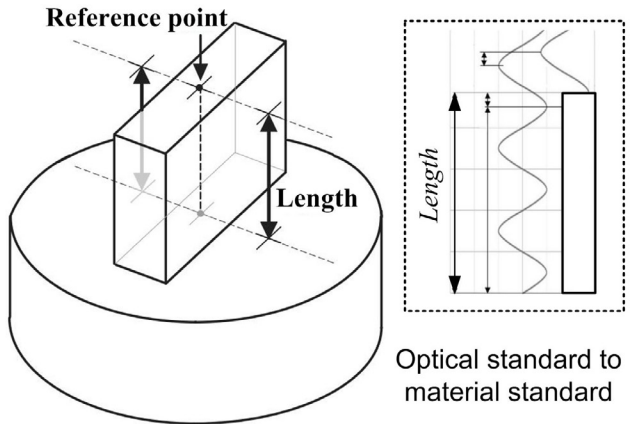


**Figure 2.** Definition of gauge block length in terms of wavelength: mechanical length is spanned by an integer number of wavelengths and remaining fraction of wavelength.

temperature, so the single frequency laser output is stabilized by balancing the intensity of two adjacent modes. In the interferometer part (figure 3(b)), a linear polarizer and a polarizing beam splitter (PBS) are used to generate two beams, one vertically polarized and the other horizontally polarized, which are propagated along the measuring arm and reference arm, respectively. In both arms, the beams pass through the quarter wave plate (QWP) twice, whose polarization state is rotated through  $\pi/2$ . In the detection and signal processing part (figure 3(c)), by using a half wave plate (HWP), a QWP, a beam splitter (BS) and two PBSs, the interferometric signals,  $i_1, i_2, i_3$  and  $i_4$  with the phases of 0,  $\pi/2$ ,  $\pi$  and  $3\pi/2$ , respectively, are detected by four photodetectors (PD). After two subtraction operations, the two quadrature signals are obtained and then converted into a displacement via bidirectional counting and fringe subdivision.

It can be seen from equation (4) that under ideal conditions, two quadrature signals,  $i_x(t)$  and  $i_y(t)$ , should have the same AC amplitude without DC offset and an exact phase difference of  $90^\circ$ . As a result, the phase  $\varphi(t)$  will be obtained by equation (5). When the measuring mirror moves by distance  $d$  during the time period of  $[t_0, t_1]$ , the phase shift  $\Delta\varphi$  is proportional to the displacement of the measuring mirror, which can be obtained by equation (6):

$$i_x(t) = A \cos \varphi(t), i_y(t) = A \sin \varphi(t) \quad (4)$$

$$\varphi(t) = \begin{cases} \arctan [i_x(t)/i_y(t)] + 2\pi N(t), & i_x(t) > 0 \\ \arctan [i_x(t)/i_y(t)] + \pi + 2\pi N(t), & i_x(t) \leqslant 0 \end{cases} \quad (5)$$

$$d = \frac{\Delta\varphi}{4\pi} \lambda = \frac{\varphi(t_1) - \varphi(t_0)}{4\pi} \lambda. \quad (6)$$

As an intensity-detection based method, homodyne interferometers usually suffer from the DC offset error which is an impediment to realizing high-speed and high-resolution measurements [52]. Using the detection and signal processing method shown in figure 3(c) and replacing the PBSs with Wollaston prisms, which have a higher extinction ratio, the DC offset error is significantly reduced [53], and the cyclic error is compensated [54]. Since the homodyne interferometer

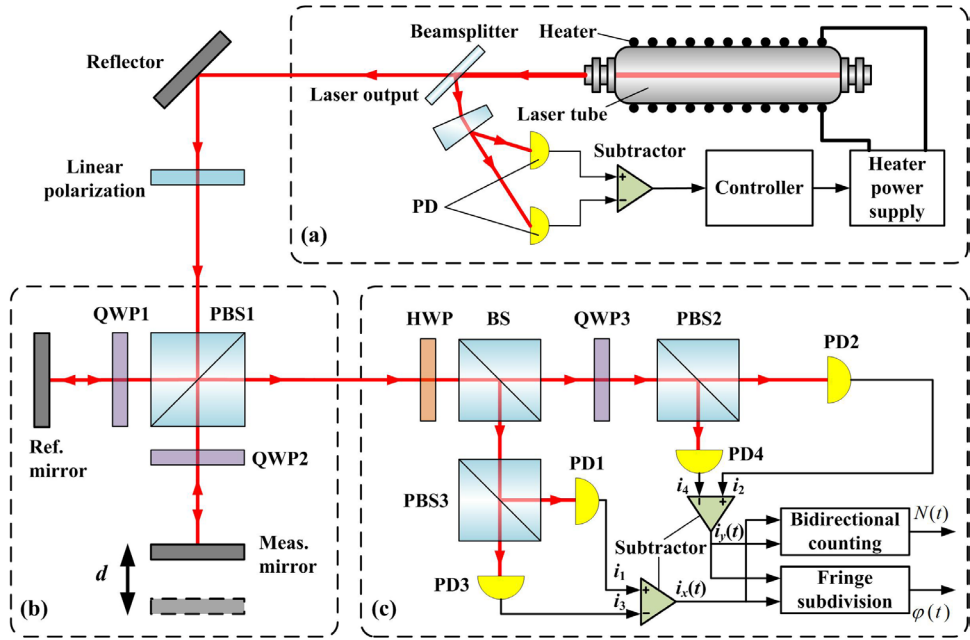


**Figure 3.** A robust laser interferometry system. (a) Stabilized single-frequency laser source. (b) Interferometer part. (c) Detection and signal processing part.

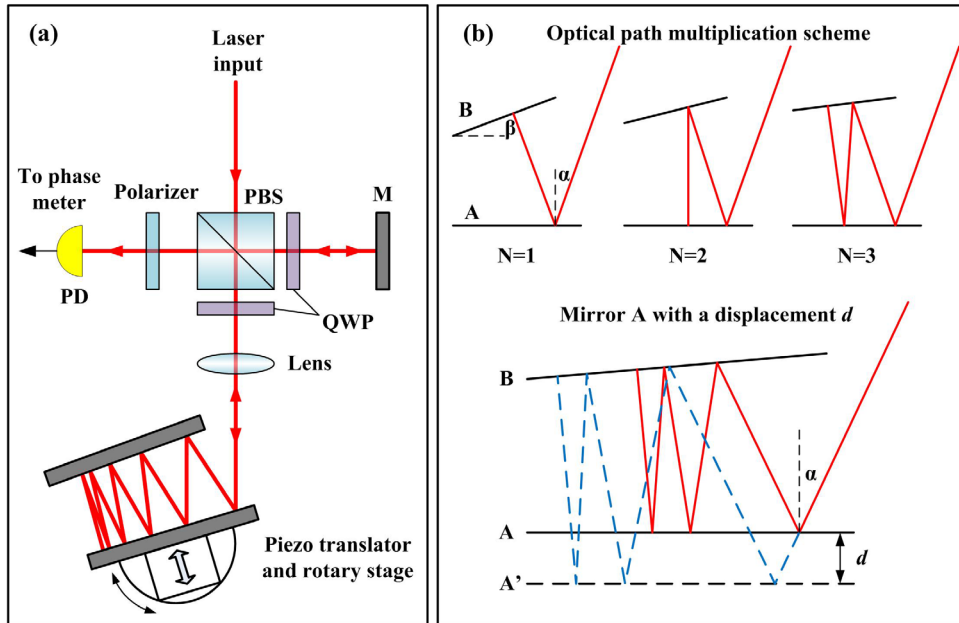


**Figure 4.** Multiple reflection interferometer. (a) Setup. (b) Measurement principle.

is very sensitive to environmental disturbances, another effective method is to add a reference interferometer as a compensator which shares the common beam arm with the measuring interferometer [55].

With the adoptions of the optical path multiplication, electronic frequency multiplication and interference fringe subdivision techniques, the measurement resolution has reached subnanometer [56, 57]. To further improve the resolution, Pisani [58] exploited a multiple reflection arrangement between two quasi-parallel mirrors to realize subpicometer resolution. Figure 4 shows the schematic of the multiple reflection interferometer. When mirror A is moved in the position  $A'$

with a displacement  $d$ , the optical path increment can be seen as the added parts below the initial mirror position, which is larger than  $d(N + 1)$ . In this experiment, by using two 50 mm diameter mirrors, a multiplication factor exceeding 100 has been obtained.

Most of the commercial laser interferometers are heterodyne interferometers [59–61], also called dual-frequency interferometers, in which the frequency difference can be generated by the Zeeman effect [62] or an acousto-optical modulator [63, 64], as shown in figure 5(a). It overcomes the shortcomings of the DC drift of the single-frequency laser, and has the advantages of low noise and strong anti-interference

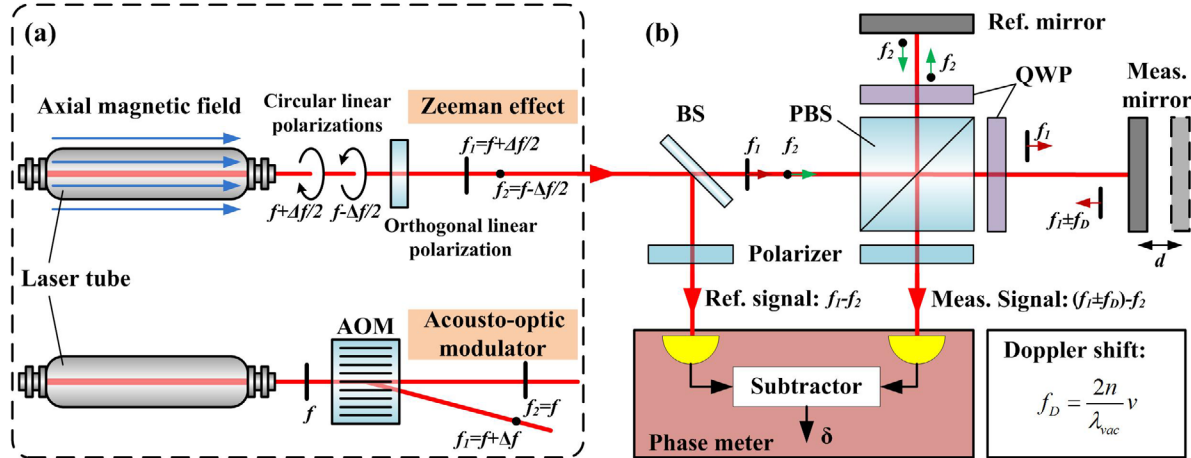


Figure 5. A common configuration of the heterodyne interferometer.

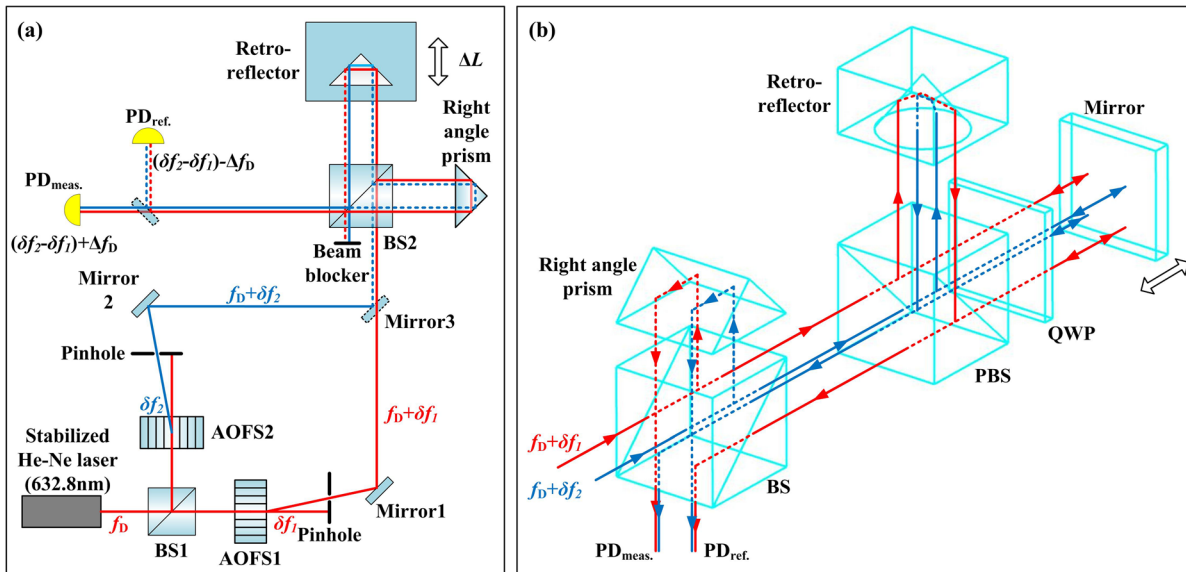


Figure 6. Optical configuration of a high-resolution heterodyne interferometer with no detectable periodic nonlinearity [70]. (a) Retro-reflector. (b) Plane mirror. Reproduced with permission from [70]. © 2010 Optical Society of America.

ability. The heterodyne interferometer uses the dual-frequency beam with a certain frequency difference  $\Delta f$  as a carrier signal, and its typical configuration is shown in figure 5(b).

The Doppler shift  $f_D$  caused by the displacement of the measuring arm makes the beat signal of the measuring and reference beam change. According to equations (7) and (8), the displacement  $d$  can be calculated by measuring the variations of phase  $\delta$  caused by  $f_D$ :

$$i(t) = A \cos [2\pi (\Delta f + f_D) t] = A \cos [2\pi \Delta f t + \delta] \quad (7)$$

$$\delta = 2\pi \int_0^t \frac{2n}{\lambda_{\text{vac}}} v dt = \frac{4\pi n}{\lambda_{\text{vac}}} d. \quad (8)$$

With the rapid development of electronic phase measurement technology, the resolution of the displacement measurement of the heterodyne interferometer has reached subnanometer [65]. When a He-Ne laser ( $\lambda = 632.8 \text{ nm}$ ) is adopted as the light source, a commercial displacement interferometer with retroreflectors, which has an optical resolution of  $\lambda/2$

(316.4 nm), can realize a displacement measurement with a  $\lambda/2048$  (0.31 nm) resolution from fringe interpolation [66]. However, the periodic nonlinearity stems from a mixed heterodyne source, misalignments and imperfect polarizing optics, and degenerates the purity of the interference signal or invokes an unexpected phase change. The nonlinear error in most commercial laser interferometers is several nanometers to dozens of nanometers, which is a decisive factor in the improvement of measurement accuracy. As a primary concern, either algorithm methods [67, 68] or two spatially separated beam interferometer configurations [69] have been developed to reduce errors from periodic nonlinearity. Joo *et al* [70] used two spatially separated beams with an offset frequency and an interferometer configuration which has no mixed states to prevent polarization mixing. Figure 6 shows a retro-reflector and plane mirror interferometer structures, and two acousto-optic frequency shifters (AOFS) are used to generate two different frequencies,  $(f_0 + \delta f_1)$  and  $(f_0 + \delta f_2)$ , from a stabilized single frequency ( $f_0$ ) source.

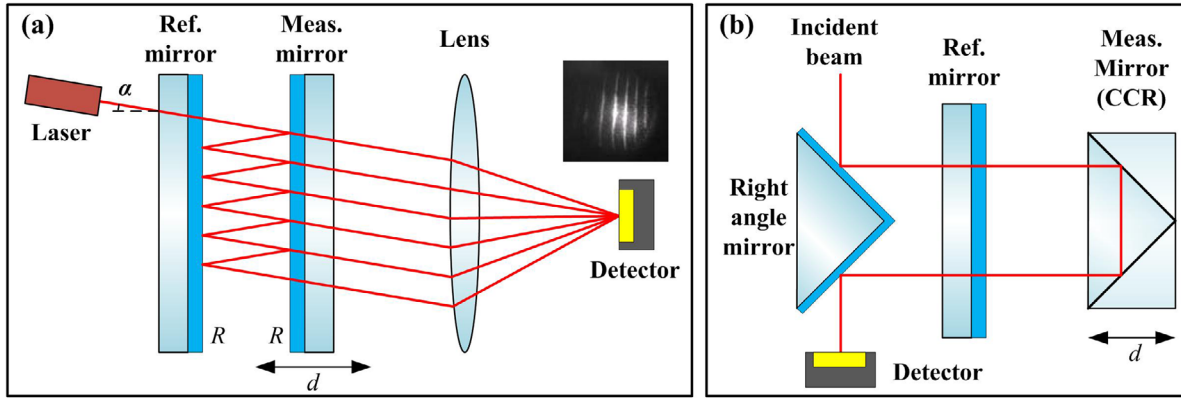


**Figure 7.** Fabry–Perot interferometer. (a) Conventional configuration. (b) Folded cavity.

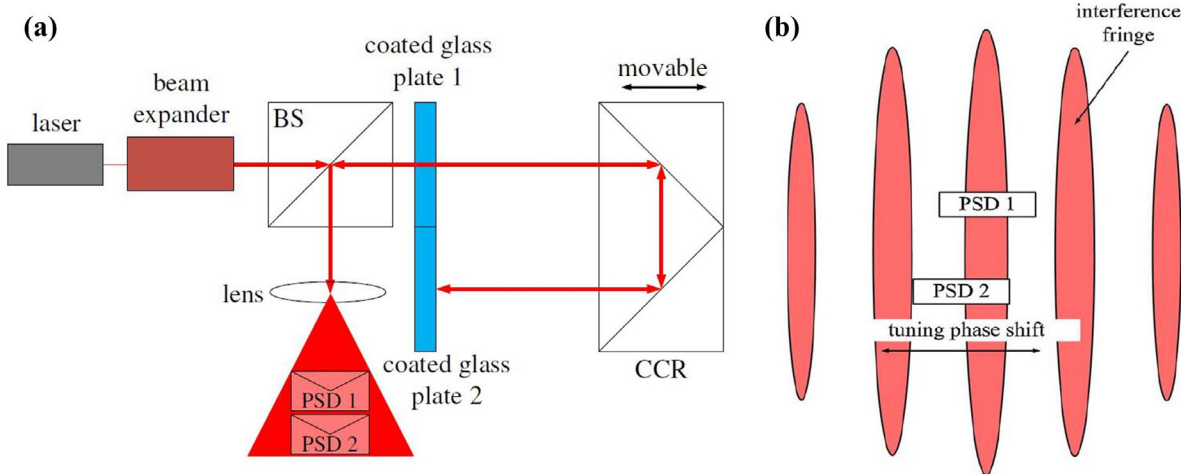


**Figure 8.** Fabry–Perot interferometer for the measuring range of up to 100 mm [78]. (a) Interferometer configuration. (b) Arrangement of the two PSDs. Reprinted from [78], Copyright 2013, with permission from Elsevier.

This arrangement is able to create a beat frequency of ( $\delta f_1 - \delta f_2$ ) without the leakage component of each beam to cause periodic nonlinearity, and the experimental results verified that the periodic nonlinearity was below the measurement noise level of 20 pm. Weichert *et al* [71] developed a heterodyne interferometer with periodic nonlinearities smaller than  $\pm 10$  pm. Yan *et al* [72] analyzed the periodic nonlinear error resulting from the misalignment of a PBS. Meanwhile, the development of the heterodyne interferometer also focuses on the superheterodyne [73], common path [74] and all fiber-based configurations [75].

**3.1.2. Dual-beam versus multi-beam interference.** Compared to the dual-beam interferometer which is sensitive to environmental disturbances, a FPI based on the multi-beam interference principle can generate extremely sharpened and high contrast fringes and can be free from the effect of the reference arm because of the common optical path [76]. As shown in figure 7(a), the incident beam with a tiny incident angle spreads into the cavity composed of the reference and measuring mirror.

In the cavity, the incident beam travelling forwards and backwards is divided into numerous transmitted beams. The intensity distribution  $I$  of the interference beam can be derived

by interference principles and is denoted as equation (5), where  $R$  means reflectivity, and the displacement  $d$  can be calculated by measuring the phase difference  $\delta$ :

$$I = I_0 \frac{(1-R)^2}{1+R^2-2R \cos \delta} \quad (9)$$

$$\delta = \frac{2dk}{\cos \alpha}, k = \frac{2\pi}{\lambda}. \quad (10)$$

The displacement measurement by FPI is more insensitive to environmental disturbances for its common optical path. However, the conventional FPI has a limited measurement range due to the non-parallelism of the reference and measuring mirror during the displacement motion. The corner cube reflector (CCR) was adopted by Rabinowitz [77] to replace the conventional measuring mirror, as shown in figure 7(b). With this folded cavity, not only has the mechanism problem (loss of alignment) been avoided, but also the measurement resolution has been improved to  $\lambda/16$ . Chang *et al* [78] developed a modified folded FPI (see figure 8), and the interferograms can be modified by changing the glass plate coated with different reflectance. The fringe spacing is adjusted to be equal to the width of the sensing area of the position sensitive detector (PSD) by regulation of the tilt angle of the coated plane mirror.

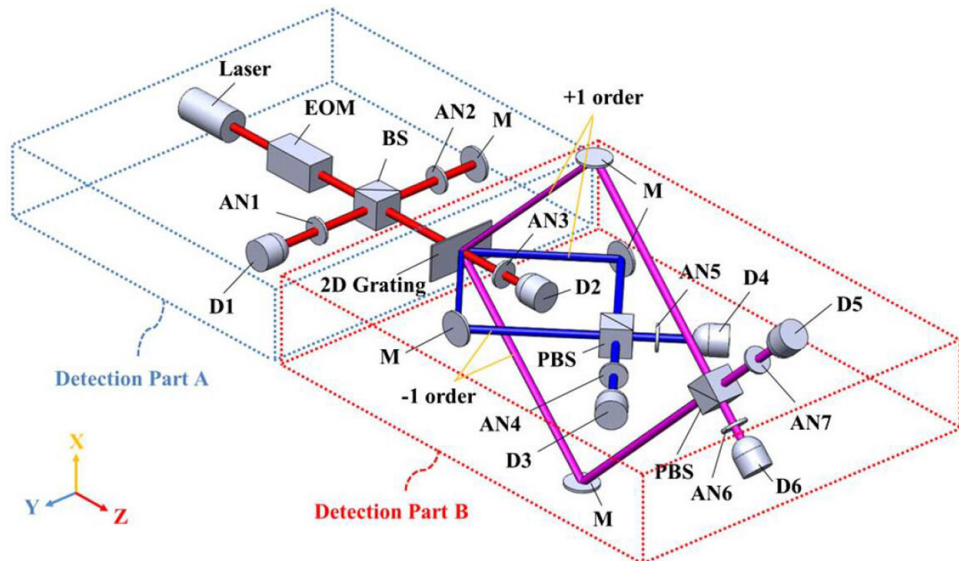


**Figure 9.** Optical configuration of the grating-based heterodyne interferometer. Reproduced with permission from [86]. © 2004 Optical Society of America.

Experiment has verified that the measuring range is larger than 100 mm and the standard deviation of the comparison experiment is within half a wavelength in the whole measuring range. Improvements are also devoted to research into light source and the design of highly compact constructions, such as the use of an optical fiber laser with a large tuning range to expand the measuring range [79], and a new optical fiber based low-finesse Fabry–Perot interferometer [80].

**3.1.3. Wavelength standard versus material constant.** High precision diffractive optical elements (DOE) provide a new perspective for interferometry when they are used as the beam splitter and the equal path interferometer is built with diffracted beams. The OPD is no longer affected by the measured variations, and some material constants of the DOE can be used as the benchmark instead of the wavelength. For instance, grating interferometry [81], whose measurement accuracy is dependent on the lithographic accuracy of the grating line and is rarely affected by the light source intensity and wavelength variation, performs well in any operating conditions. The grating groove density and the subdivision multiples control the resolution. The traceability is derived by the grating period. The precision of laser grating interferometers has reached the nanometer level and even higher [82]. The resolution of the general laser grating polarization interferometer is  $\sim 10$  nm [83], and the resolution of the laser grating heterodyne interferometer can reach 1 nm [84]. Some grating rulers in the measurement region of 100 mm can reach a resolution of 1 nm [85]. Figure 9 shows a grating-based heterodyne configuration for 3-DOF (degree of freedom) displacement measurement [86]. When the heterodyne light beam is perpendicular to a transmission-type 2D grating, two detection configurations for simultaneously measuring 2-DOF in-plane and 1-DOF out-of-plane displacements can be obtained without changing the optical arrangement.

Similarly, XRI, which was proposed by Bonse and Hart [87, 88], uses the crystal lattice of single crystal silicon as the

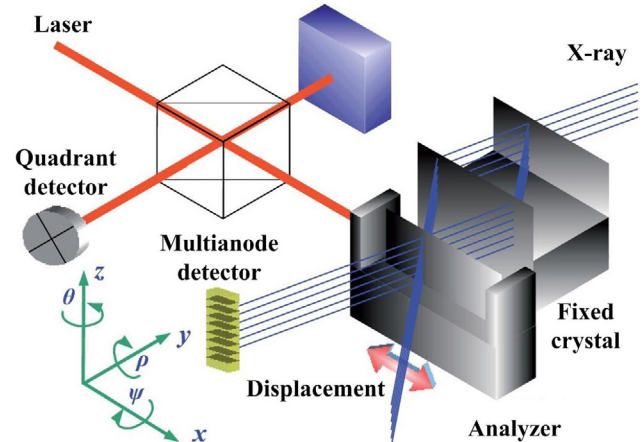


**Figure 10.** Combined x-ray and optical interferometer. Reproduced from [90]. © IOP Publishing Ltd. All rights reserved.

grating where x-rays are diffracted. It derives its traceability from the lattice constant which is in the order of subnanometer, and hence it is capable of subatomic metrology [36, 89]. A combined optical and x-ray interferometer (COXI) is shown in figure 10, in which the ray paths in XRI are similar to those in a Mach–Zehnder interferometer. The diffracting elements are three thin uniformly-spaced crystal lamellae and details of the configuration of the x-ray optics are given in [90]. When the analyzer moves with respect to the other two crystals, the intensity of the output light varies periodically in a sinusoidal fashion. In this way, the displacement of the analyzer can be obtained by counting the fringe period and multiplying by the spacing of the crystallographic plane. If a (220) plane, whose spacing is 0.192 nm, is used as the diffraction grating, the measurement accuracy can reach picometer level while the range (usually less than 10  $\mu$ m) is limited by the size of the crystal. The Physikalisch-Technische Bundesanstalt (PTB) has developed a COXI for the ultra highly accurate measurement of the silicon lattice spacing, and the traceability to the meter is obtained via calibrations of the lattice constant

and laser frequency [91]. The laser interferometer produces a relatively coarse, and very precise, scale that can be directly traced to the length standard, and the XRI subdivides each graduation of this scale into over 800 precisely equal parts, and each is equal to the silicon lattice spacing of  $0.192 \pm 1.2 \times 10^{-8}$  nm. However, the disadvantages of XRI are the manufacturing difficulties of single crystal silicon, low measuring speed, small range, as well as measurement error due to the elastic deformation and mechanical processing.

### 3.2. Distance measurement

**3.2.1. Self-mixing interferometry (SMI).** In contrast to conventional laser interferometry, SMI, in which the interference occurs inside the laser cavity, works without a reference path outside the laser cavity [92]. A low-cost and compact diode laser [93] is usually used as the source of the SMI, which is due to the fact [94, 95] that any reflection coming from the object will modulate the laser output when it re-enters the diode cavity. This happens as the laser must be stable in both the internal and external cavities. The external cavity contains the object and the internal cavity. The modulation is usually detected from the amplitude variation by recording the monitor PD in the laser head. Affected by the feedback, the output laser power oscillates with the object moving, and the oscillation period corresponds to an object displacement of  $\lambda/2$ . The diode laser SMI has been applied to the distance measurement, because the diode laser has high sensitivity and power, and the interferometer has a simple configuration which reduces the loss to laser power. Shinohara *et al* [96] proposed the method for distance measurement using a self-mixing laser diode. The interferometer detects the averaged mode hop time interval of successive external mode hops by the backscattered light from an object; this system has a measurement error of  $\pm 0.15\%$  in the range of 0.2 to 1 m. From this work, the laser feedback effect in diode lasers has been widely used for measuring absolute distance.

Diode laser SMIs have a pronounced property that a small variation of the laser driving current can result in an approximately linear response to the laser working frequency [97]. Using this property, the periodic modulation of the driving current produces the frequency sweeping for the diode laser output. A precise distance measurement can be realized using the injected current reshaping in a SMI based on the vertical-cavity surface-emitting laser (VCSEL) invented by Kou *et al* [98]. The wavelength decrease corresponds to an object moving away from the laser source, while the increase to an object moving toward the source. The tuning current taking a sawtooth shape is used to drive VCSEL to show the beat frequency change. The relationship between the laser wavelength and the frequency, with respect to the injected current, is studied. Each divided frequency is calculated for an injected current, and the non-linearity is eliminated. Thus the injected current is reshaped. This method is valid for reducing the nonlinearity in current tuning, and the distance measurement resolution is increased to 20  $\mu\text{m}$  within the range 2.4 to 20.4 cm [98]. Moench *et al*

[99], Michalzik [100], and Gouaux *et al* [101] also explored the VCSEL-SMI using the modulation of the working current. Guo *et al* [102] put forward a method adopting a double modulation technique for absolute distance measurement. The laser intensity and the phase are both modulated to improve the resolution. The absolute distance has been measured with  $\pm 0.3$  mm resolution within the range of 277–477 mm.

**3.2.2. Multi-wavelength interferometry (MWI) and frequency-sweeping interferometry (FSI).** Polhemus [103] may be regarded as the pioneer who discussed, in 1973, the two-wavelength technique for interferometric testing under static conditions. In a single wavelength interferometer, the optical path difference (OPD) should be smaller than  $\lambda/2$  for absolute measurement because of the  $2\pi$  phase ambiguity. When OPD is larger than or equal to  $\lambda/2$ , a fringe counting procedure is needed and the interferometer must keep a continuous line of sight during the movement of the measuring object. In MWI, the interference phase at the so-called synthetic wavelength can be directly calculated by simultaneously measuring phase at both wavelengths [104]. As the two wavelengths must be optically separated before detection, it can be applied only for relatively large wavelength differences and thus only small synthetic wavelengths can be obtained. Super-heterodyne detection, introduced by Dandliker *et al* [105], makes high-resolution measurements available at arbitrary synthetic wavelengths  $\Lambda$  without the need for interferometric stability at the wavelengths or separation of these wavelengths optically. This is of great significance for range finding and distance measurement with submillimeter resolution.

With half of this large synthetic wavelength, the fringe counting is unnecessary. However, the measurement uncertainty is increased when the distance is measured using the synthetic wavelength [106]. Cheng and Wyant [107] proposed a method to decrease the uncertainty of two-wavelength interferometry by introducing the phase data of a third wavelength. Using more than two wavelengths an extension of the unambiguous range with low uncertainty is achievable. The difference between two phases  $\Phi_i$  and  $\Phi_j$  from the wavelengths  $\lambda_i$  and  $\lambda_j$  is given by

$$\Phi_i - \Phi_j = \left( \frac{2\pi}{\lambda_i} - \frac{2\pi}{\lambda_j} \right) 2 \cdot \text{OPD} = \frac{4\pi}{\Lambda_{ij}} \text{OPD}, \Lambda_{ij} = \frac{\lambda_j \lambda_i}{\lambda_j - \lambda_i}. \quad (11)$$

A three-wavelength interferometer (figure 11) that uses three laser diodes was developed by Meiners-Hagen *et al* [108]. The interferometric signals from these three sources can be collected simultaneously with one photodetector using the lock-in technique [109]. In this case, the larger synthetic wavelength results in a measuring range of  $\Lambda_{23}/2$  ( $\approx 145 \mu\text{m}$ ), and the result is then used to determine the fringe order of the smaller synthetic wavelength (14  $\mu\text{m}$ ). Doppler-based technique MWI is also available for moving objects [110]. Four and more wavelengths are used for further improvements [111–113].

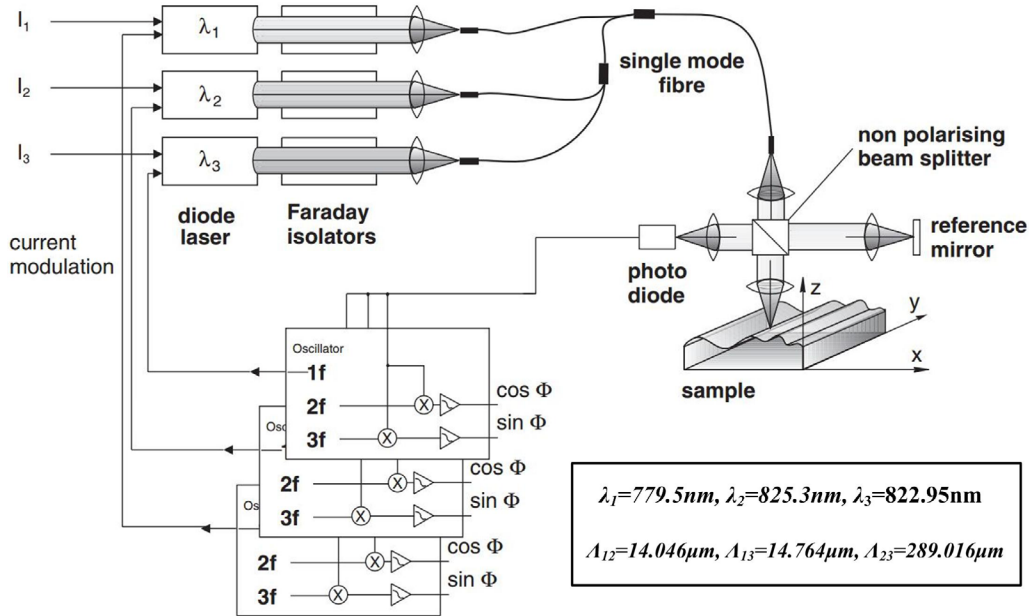


**Figure 11.** A three-wavelength interferometer. Three laser diodes are coupled into one single mode fiber. Reproduced from [108]. © IOP Publishing Ltd. All rights reserved.

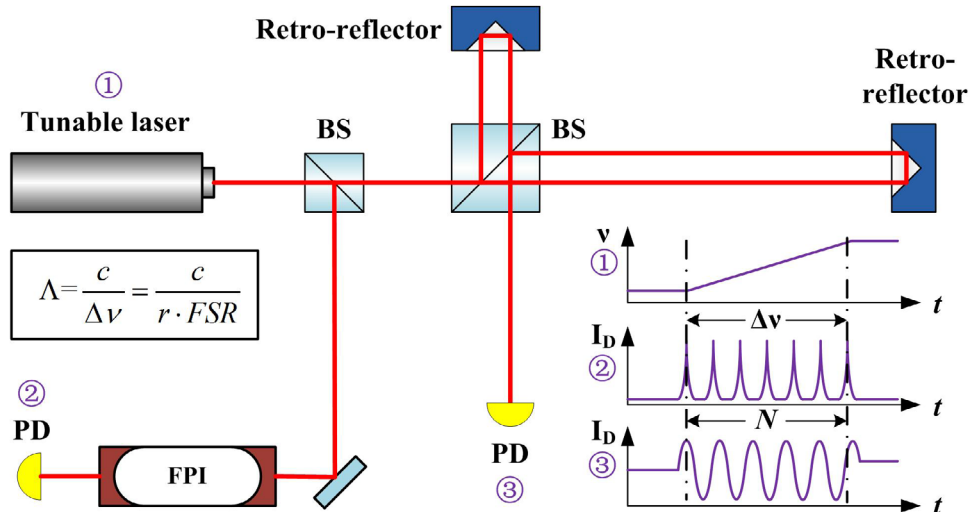


**Figure 12.** FSI setup. The sweep range measurement is obtained by multiplying the FP free spectral range (FSR) by the number  $r$  of resonances detected.

To further increase the measuring range, more wavelengths are required in the MWI whose beams have to be aligned on the same path and detected simultaneously. This arrangement will become complex and be easily affected by the thermal and mechanical drift. The effort can be reduced by FSI [114], which was not explored in detail until the emergence of tunable lasers and external-cavity diode lasers (ECDL). These laser sources can provide a range of wavelengths, from infrared to blue light, by varying the injection current. The generation of the synthetic wavelengths in FSI is based on frequency sweeping the laser source within a given sweep range [115–117]. As the frequency sweeps, detectors record synthetic wavelength maxima without ambiguity, rendering it particularly useful for large measuring ranges. However, the resolution is usually limited to a

few micrometers because it is very sensitive to the distance variations during the sweeping.

Compared to MWI, FSI does not need two or more independent stabilized and well-known lasers, and relies only on a tunable laser and a frequency-sweep range measurement system (using a FPI). As shown in figure 12, Cabral and Rebordao [118] presented a theoretical model of FSI and its uncertainty evaluation with a prototype sensor composed of a mode-hop-free frequency-sweep ECDL, a high-finesse FPI, homodyne detection, and data processing. While the frequency sweeps (and the FPI is measuring the sweep), the PD counts the number of fringe circles, including the fringe fraction, from the beginning to the end of the sweep, without ambiguity.

The measured OPD is given by equation (8), where  $N$  is the number of fringes and  $n$  the refractive index of the propagation

medium. The results have revealed that the accuracy is  $\sim 10 \mu\text{m}$  for distances up to 1 m, at an affordable complexity:

$$\text{OPD} = \frac{N}{2} \cdot \frac{\Lambda}{n} = \frac{N}{2} \cdot \frac{c}{r \cdot \text{FSR} \cdot n}. \quad (12)$$

A movement of the object over one wavelength can result in large consequences since it is regarded as the movement over one synthetic wavelength. To solve this problem, a second laser source is usually introduced to decrease the sensitivity to movements of the order of the synthetic wavelength itself [119], or to compensate the movement errors with algorithms, e.g. combining four consecutive phase measurements instead of two [120].

Generally, a number of synthetic wavelengths are required in FSI, and this will also lead to a low measurement speed. A revolution in absolute distance measurement is the advent of the optical comb [121], which can eradicate an equispaced ultrashort pulse sequence with a broad spectrum comprising discrete, uniform mode-spacing narrow lines. When its mode frequencies are linked to a frequency standard, it becomes an ultra-accurate ruler in space, time and frequency domains [122, 123]. Since the first work was carried out by Minoshima *et al* [124], various methods have been put forward for such research, which have been comprehensively reviewed by Jin [125]. Among them, using the adjacent pulse repetition interval length (APRIL) as a scale to realize absolute distance measurement is more effective [126–128]. The accuracy relates to the relative positions of the two overlapped pulses, whose peak position of interferogram envelope can be used for the pulse-to-pulse alignment [129, 130]. It can achieve micrometer-, or even submicrometer-, level alignment, however, the accuracy is suppressed by the intensity noise of the interferogram envelope. To improve the accuracy, several works have been carried out on improving the peak-finding method [131] or linking the peak-finding with the interferometric phase [132].

**3.2.3. Low-coherence interferometry.** From an optical point of view, we can classify the low-coherence interferometric techniques as either time domain WLI [133, 134] or frequency domain optical coherence tomography (OCT) [135, 136]. The latter emphasizes the utility of tomography, and is mainly used in biological and medical applications. The time domain WLI, whose traceability is derived by the positioning mechanism [137], can be used as a displacement or distance sensor [138–140]. The position of the object is derived by scanning the reference mirror to find the point at which the OPD becomes closer to zero, the maximum fringe contrast. The light source can be a visible or near-infrared diode, or incandescent source with a spectral width of up to hundreds of nanometers. The coherence length  $l_c$  of these sources is normally in the micrometer level, and is given by  $l_c = \lambda^2/\Delta\lambda$ , where  $\lambda$  and  $\Delta\lambda$  are the central wavelength and the spectral width, respectively [12]. The recently developed fiber-coupled super-luminescent diodes (SLEDs) are particularly attractive in practical applications. Pavlicek and Hausler [138] developed a fiber-optic distance sensor based on WLI, as shown in figure 13, which is designed for in-process measurement.

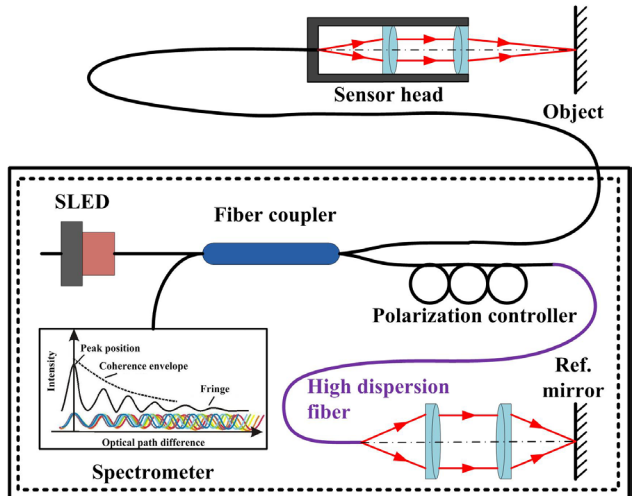


**Figure 13.** A WLI fiber-optic sensor for in-process measurement. Reproduced with permission from [138]. © 2005 Optical Society of America.

As a full scan of the reference mirror needs to be performed in order to determine the object distance, it is a relatively slow process and only available for measuring distances to quasi-static objects. WLI can, theoretically, measure distances with an accuracy of subwavelength [141]; however, practically, some factors such as signal-to-noise ratio and the mechanical drift of the scanner will limit the accuracy to  $1 \mu\text{m}$ . Recently, a point-to-point absolute distance measurement was realized, by Winarno *et al* [142], using tandem low-coherence interferometry. Taking a He–Ne laser interferometer as a reference length standard, an internal distance of up to 100 mm was measured with an uncertainty of 178 nm. This is also available for gauge block interferometry [143].

## 4. Interferometric techniques for surface measurement

### 4.1. Full-field interferometry

**4.1.1. Laser phase-shifting interferometry (PSI).** A significant step was the use of detector arrays, such as a CCD camera, to substitute for conventional methods of recording and analyzing interferograms, which made fast areal measurement possible. Since Carre [144] introduced the temporal phase-shift measurement technology in 1966, and after a further development by Burning [145] in 1974, PSI has been widely studied. PSI records several interferograms where the phase of the two adjacent interferograms is changed by a known amount and direction. The wavefront phase and its sign can be obtained from the variation of intensity at each pixel between interference images. Compared to the static interferogram analysis, PSI performs much higher spatial resolution and measurement accuracy, and shows good results from low contrast fringes. Since the phase is calculated independently at each pixel, the intensity variations, the pixel-to-pixel nonlinear variation and the source distribution no longer affect the phase accuracy. PSI has been adapted to various interferometer types such as Twyman–Green, Fizeau, Mach–Zehnder, and also common

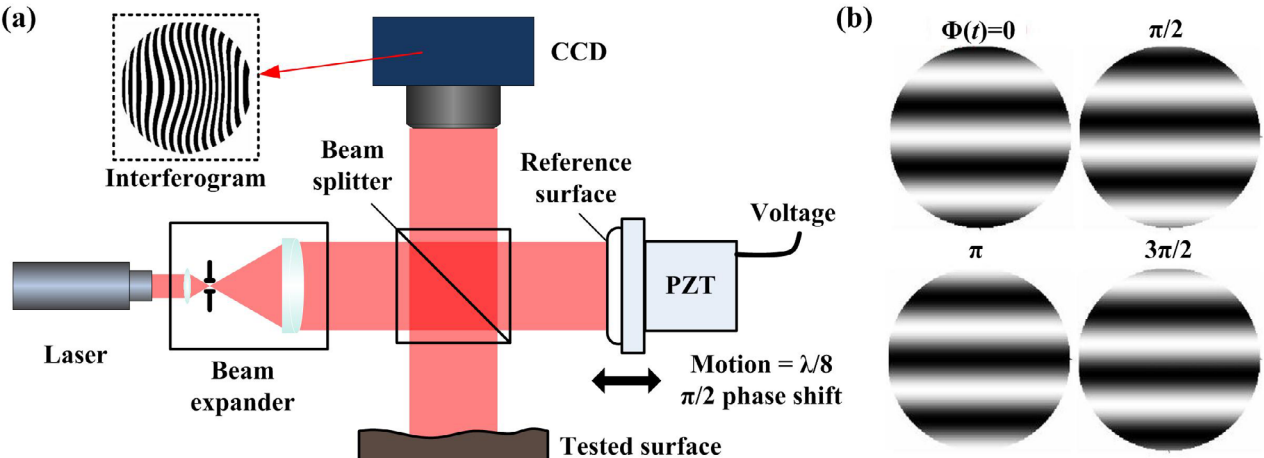


**Figure 14.** (a) Setup of PSI. (b) Phase shift interferogram.

path configurations such as point diffraction and lateral shearing interferometers [146, 147].

It can be considered that the interferometer illuminated full-field measurement with a collimated wavefront in the Twyman–Green variant, as illustrated in figure 14(a). Usually a laser is used as the light source, and a beam expander is used to broaden the spot size to achieve large area full-field information acquisition. The interference fringe is deformed since it is modulated by the fluctuation of the tested surface. The phase shifting is generated by a mechanical motion of a piezoelectric ceramic transducer (PZT), and the most common phase shift between images is  $\pi/2$ , which is equivalent to moving the reference mirror  $\lambda/8$ , as shown in figure 14(b).

According to the theory of dual-beam interference, the intensity distribution  $I(x, y)$  of the interference field can be expressed as (9), and the height  $h(x, y)$  can be calculated by (10) when we get the phase  $\Phi(x, y)$  to be measured:

$$I(x, y) = I_{dc}(x, y) + I_{ac}(x, y) \cos[\Phi(x, y) + \Phi(t)], \quad (13)$$

$$\begin{aligned} I_1(x, y) &= I_{dc} + I_{ac} \cos[\Phi(x, y)], \Phi(t) = 0 \\ I_2(x, y) &= I_{dc} - I_{ac} \sin[\Phi(x, y)], \Phi(t) = \pi/2 \\ I_3(x, y) &= I_{dc} - I_{ac} \cos[\Phi(x, y)], \Phi(t) = \pi \\ I_4(x, y) &= I_{dc} + I_{ac} \sin[\Phi(x, y)], \Phi(t) = 3\pi/2, \end{aligned} \quad (14)$$

$$\Phi(x, y) = \tan^{-1} \left( \frac{I_4 - I_2}{I_1 - I_3} \right), \quad (15)$$

$$\Phi(x, y) = \tan^{-1} \left( \frac{2(I_2 - I_4)}{2I_3 - I_5 - I_1} \right), \quad (16)$$

where  $I_{dc}$  is the background intensity and  $I_{ac}$  is the fringe amplitude. The phase difference between images is  $\Phi(t)$ , and the most common value is  $\pi/2$ , see (10). The irradiance  $I(x, y)$  can be obtained at each pixel. As in (11), the minimum number of phase shifts needed to determine  $\Phi(x, y)$  is three [148], and a fourth interferogram helps reduce the error result from incorrect phase shifts. Further improvement occurs by the fifth interferogram, see (12), where additional  $\Phi(t) = 2\pi$  [147, 149], but this algorithm is much less sensitive to miscalibration of the phase shifter. The calculated phase  $\Phi(x, y)$  can be converted

to optical path difference (OPD), which is then converted to the corresponding point height of the tested surface:

$$h(x, y) = \frac{\text{OPD}(x, y)}{2} = \frac{\lambda}{2\pi} \Phi(x, y). \quad (17)$$

PSI adopts a monochromatic source and is usually used in the analysis of very smooth surfaces because it is characterized by subnanometer resolution [150]. However, it suffers from phase ambiguity, which limits PSI serviceability to a surface discontinuity lower than  $\lambda/4$  [151]. In order to overcome this problem, MWI, as discussed in section 2.2, has been applied to extend the height difference limitation effectively. In this system, two or more wavelengths are used to increase the dynamic range and to keep the resolution constant simultaneously [152–154]. However, this is only applicable so long as the phase difference between the two wavelengths across the surface discontinuity is not less than the uncertainty in the measured phase values. A better way to broaden the measuring range further is to add more wavelengths [155], and further improvement can be realized when bandwidth light source is adopted [156]. Measurement errors can be easily introduced since the image acquisition of a series of interferograms is very sensitive to environmental vibrations, and a simultaneous PSI method was adopted to meet this problem, as reported in [157]. Nevertheless, monochromatic PSI is still an indispensable method for ultra-precision measurement and its development mainly depends on the progress of phase shift extraction algorithms [158–163].

When it comes to in-process or on-machine measurements, however, multiple frames of data are required over many milliseconds, which means vibration and turbulence have enough time to degrade the measurement results. A better approach for reducing these effects is to capture all the phase shifting frames that fall on a single CCD camera at once [164]. As shown in figure 15, a holographic optical element (HOE) is used to split interferograms into four separate beams. The four beams pass through a phase shifting mask and a polarizer with its transmission axis at  $\pi/4$  in the direction of the polarization of the test and reference beams placed in front of the CCD array. In this way a single detector array captures all four phase-shifted interferograms in a single shot.

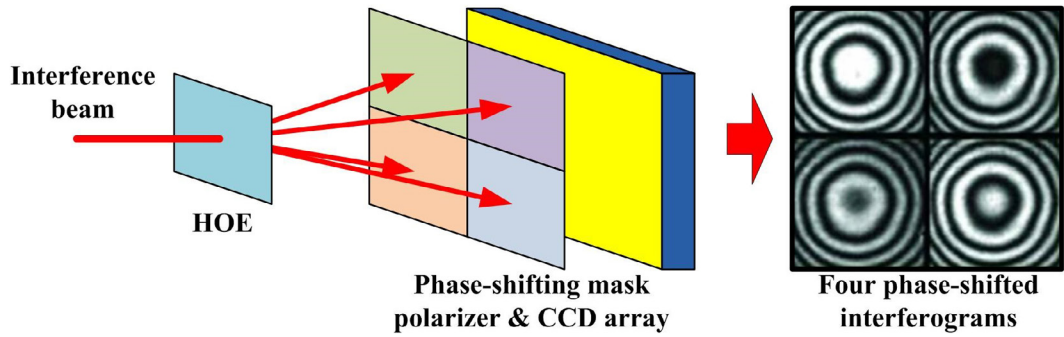


**Figure 15.** A single-shot detector to capture four separate, phase-shifted interferograms.

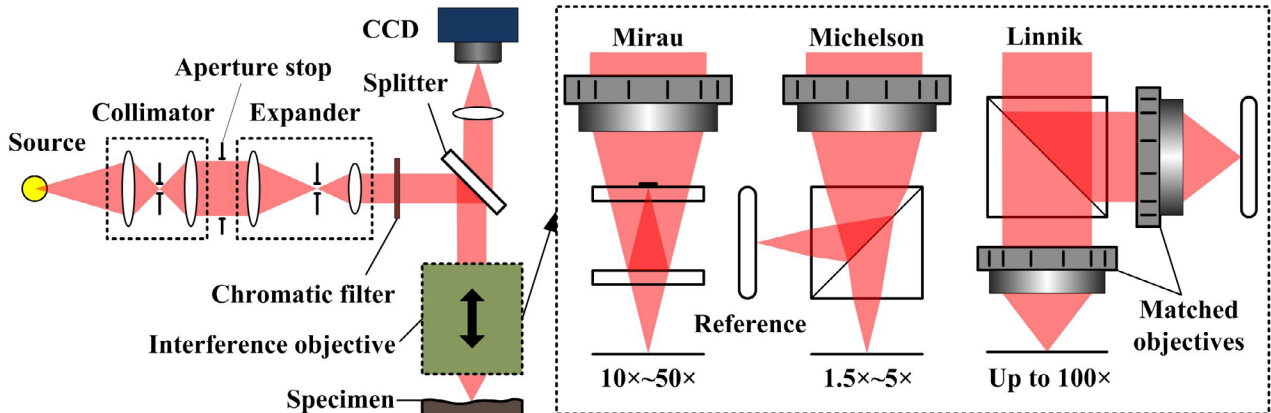


**Figure 16.** Typical configurations of microscopic interferometers.

**4.1.2. Microscopic interferometry.** With the combination of interferometers and microscopes, we can obtain high lateral resolution [165, 166]. Optical imaging has significant potential for 3D full-field measurement in that tens of thousands of points of cloud data can be obtained at one time without lateral scanning [167]. Monochromatic PSI [168] and vertical scanning WLI (VSWLI) are the two main methods in the full-field microscopic interferometry which provide higher magnification, resolution and intuitive measurement results. PSI microscopy has offered a fast, even real-time and areal measurement method for mapping surface microstructures in 3D with excellent vertical resolution by analyzing the deformation of the interference fringes [169, 170]. The light source adopted in a PSI microscope is generally a spectrally filtered white light source with a coherence length of tens of micrometers. This gives the advantage of eliminating spurious fringes introduced from other surfaces when the coherence length is long enough, so that fairly large surface topography variations can be distinguished [171]. In the measurement process, we can see the interference fringes on the tested surface deviate from flatness. Generally, this information is obtained by observing the direction that the fringes move when the reference surface is pushed. The lateral resolution is limited by the optical resolution, as with any optical microscope [172], and some improvements are under investigation to overcome the diffraction limit [173, 174]. A simple way is to use data acquired during sub-pixel positioning and subsequently deconvolved via standard image enhancement algorithms [173].

Schematics of the operation principle and construction of typical microscopic interferometers are shown in figure 16. Mirau, Michelson and Linnik interferometric objectives are three of the different objectives used in a PSI microscope, and each of them is applicable to different magnification ranges [175]. Mirau, as a common path interference microscope, has a central obscuration due to the reference mirror, and its magnification is generally around 10 to 50 times. Michelson is an optical-path-splitting interference microscope, and its magnification is only about 1.5 to 5 times, since the working distance is limited by the size of the beam splitter. Linnik, similar to the structure of Michelson, is suitable for large magnifications of up to 100 times since the two same microscope objectives are respectively added in the measuring and reference path, but needs two perfectly matched objectives, which makes it expensive. One major shortcoming of all microscopic interferometers is that any variation in the phase change on reflection due to different specimen composition will be interpreted as a false height variation [176]. Additionally, the maximum step height between adjacent pixels that can be clearly distinguished by a PSI microscope is  $\lambda_c/4$ , where  $\lambda_c$  refers to the center wavelength of the filter.

The first WLI-based automatic 3D surface topography measurement system was proposed by Balasubramanian in 1983 [177]. According to the large spectral bandwidth of the white light source, the coherence length is very short (a few micrometers), and good contrast interference fringes will occur only when the two paths of the interferometer are almost equal in length. Applying WLI to microscopic interferometers

to overcome the problem of height ambiguity was a significant breakthrough in the development of microscopic interferometry. VSWLI microscopy uses the characteristics of full spectrum white light interferograms to measure the surface micro topography with a discontinuous profile [178, 179]. To obtain the surface topography, the positions with zero OPD of all points on the surface are recorded. When the optical structure and accuracy of the scanning mechanism have been determined, the positioning accuracy of the zero OPD point is directly related to the spectral width of the light source and the processing algorithm of the interference signal. Tian *et al* [180] compared the key algorithms, namely weight center, phase shift, frequency domain analysis, and coherent correlation, to determine the zero OPD position in VSWLI. Lei *et al* [181] employed correlation analysis of WLI envelope curves and a multi-reference position based phase solution method for robust and high precision surface recovery.

Since the white light interferogram includes both fringe and coherence envelope features, the improved approach is to combine PSI and VSWLI to achieve high-accuracy large-range measurement [182, 183]. A coarse positioning is carried out by using VSWLI, and then a precision phase calculation is executed by PSI. Both coarse and precision data are finally combined to express the position of the measured point. In principle the height difference of the discontinuous surface measured by the VSWLI microscope is unlimited but is only figured out by the travel range of the scanner. This travel range is in the order of millimeters and depends on the working distance of the objective, which performs an important role in the VSWLI system [184, 185]. 3D image stitching methods are used to enlarge the lateral measuring range [186, 187], and this technique is discussed in section 4.2.4. The combination of WLI with a color CCD camera has also been a research hotspot in recent years, which makes the MWI as simple as the one single wavelength case [188–191].

A series of error sources such as mechanical vibrations and optical noises as well as aliasing of fringe orders caused by the low-reflection will also lead to wrong detections of coherence peaks, which should be under consideration to improve the robustness of the algorithms [192]. Tereschenko *et al* [193] developed a close-to-machine system that integrates a real-time distance sensor with the VSWLI. The distance sensor is a laser interferometer and monitors any distance variation during the measurement process of VSWLI with a high temporal resolution. With the knowledge of the real-time distance variations the error on the white-light interferograms can be compensated, and thus it can work in the presence of environmental vibrations.

**4.1.3. Macroscopic surface measurement.** Full-field interferometry extracts the surface geometry by interpreting the interferogram between a wave reflected from the surface under test and a reference wave [21]. Digital holographic interferometry (DHI) uses holography (invented by Gabor in 1948 [194] as a method to store and reconstruct whole optical fields including both intensity and phase) to measure small deformations with single wavelength [195]. In multi-wavelength implementations, it is used to perform dimensional metrology

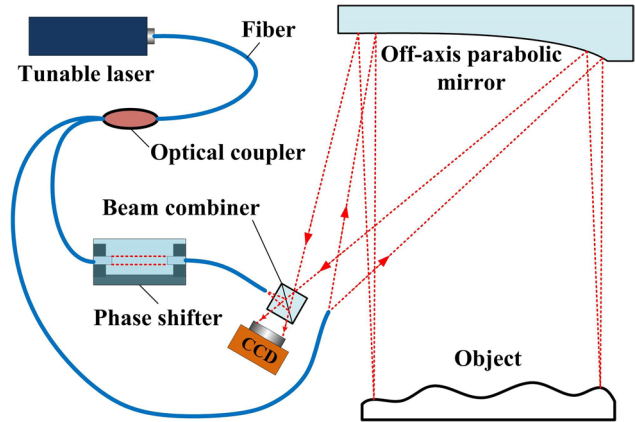


Figure 17. The optical arrangement of a large-aperture DHI.

for large parts and assemblies and to detect larger surface defects [196–198]. Figure 17 illustrates a large-aperture DHI. In this arrangement, an off-axis parabolic mirror is set up to expand and collimate the light beam, and the CCD is used to record the phase-shifted digital holograms which are further used for 3D recovery. The optical coupler divides the laser output into reference and measuring arms. The reference arm includes a phase shifter that allows the phase of the reference beam to be shifted with respect to the phase of the object wavefront [197].

However, the reference and measured wavefront cannot be much different because the fringes will become too dense to distinguish. This limits the measured surfaces to those that are nearly flat or spherical in most configurations, or it needs a very complicated configuration and the adoption of a custom computer-generated hologram (CGH) which is very difficult to fabricate and is expensive. Therefore, these methods are not available for surfaces with large curvature, e.g. complex aspherics and freeform surfaces. Lateral shearing interferometry [199–203] has the superiority that the reference wavefront is generated by duplicating the measurement wavefront and displacing it laterally by a small amount, so the fringe density is kept low and measurable. The interferogram directly reveals the slope profile of the measured surface, and then the height profile is calculated by integration.

#### 4.2. Profile measurement

**4.2.1. Point-wise mechanical scanning.** Traditional interferometers are adopted only to measure the displacement or distance point by point so as to describe the surface profilometry. The earliest interferometric profiler, proposed by Sommargren [204], adopted single point data acquisition and a mechanical scanner to achieve surface profilometry. Figure 18 shows a point scanning heterodyne interferometer using rotary point scanning for quantitative roughness measurements, and the specimen rotates on a stage to draw a circular profile [205].

One of the two coherent beams with subtle frequency difference is used as the measuring beam and is focused on the measured surface through the microscopic objective; the other beam is used as the reference beam and its path remains unchanged. The OPD between the measuring and reference

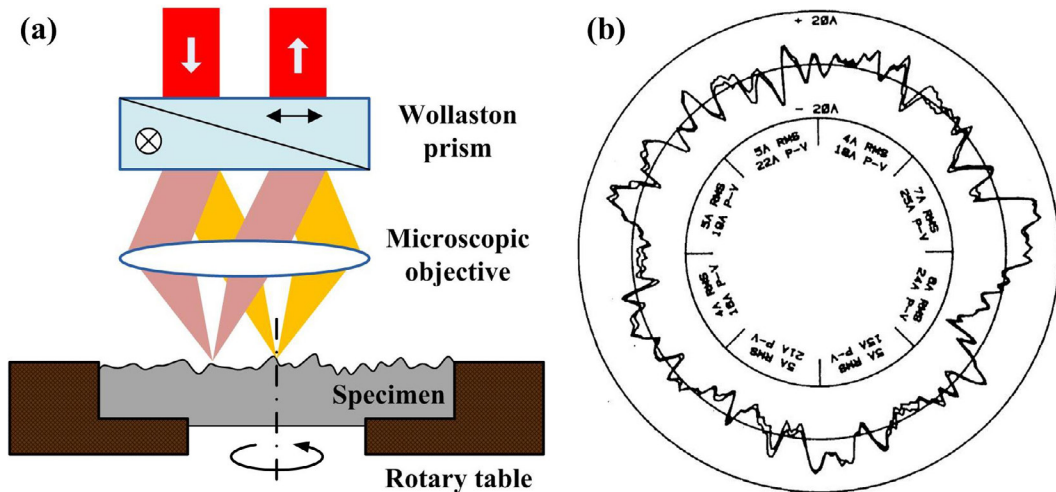


**Figure 18.** Point scanning heterodyne interferometer. (a) Rotary stage setup. (b) Circular profile of surface topography heights. Reproduced with permission from [205]. © 1981 Optical Society of America.

beams varies with the change of surface height, and the height of the surface will be obtained by phase comparison. These heterodyne phase detection principle based methods have wide applications [206–209]. Some adopt acousto-optic modulators [210–212] to obtain frequency differences between the measuring and reference beams while others employ oscillating gratings [213].

Fiber optic sensing technology [134, 214–216] provides the basis for interferometers that can produce sensors with unique characteristics such as compactness, multiplexing, remote sensing, high flexibility, immunity to electromagnetic interference, and it has been widely used for modern on-line metrology. Lin *et al* [217] proposed a self-reference multiplexed fiber interferometer using a tunable laser and fiber Bragg grating, which can be applied in both displacement measurement and on-line surface metrology. Further related research has been reported [218–220]. Martin *et al* [221] reported a double interferometer structure with a wavelength-scanning probe based on a system described in [222] which performs active stabilization against the effects of temperature drift and vibration.

Since the methods mentioned above still suffer from phase ambiguity which results in a limited vertical measuring range, the MWI based absolute distance measurement methods have been widely applied to increase the measuring range [223]. The multi-wavelength techniques can be used for 2D profilometry, with 3D information available by lateral scanning [224, 225]. Combined with precision translation or rotary stages, MWI is a feasible technique for the complex aspheric surfaces that are not easily adapted in full-field interferometry [226]. Figure 19 shows a newly developed scanning metrology platform based on MWI absolute distance measurement technology [227]. The distance sensor 1 directed at the freeform is in this case preferably configured as a multi-wavelength sensor, which determines an absolute distance between the sensor head and a selected point on the object. The possible rotationally dependent positional inaccuracies of the distance sensors 1 and 2 can be compensated for precisely by the sensor 2 by virtue of measuring a second distance in relation to the reference face 5. The position of the holder in relation

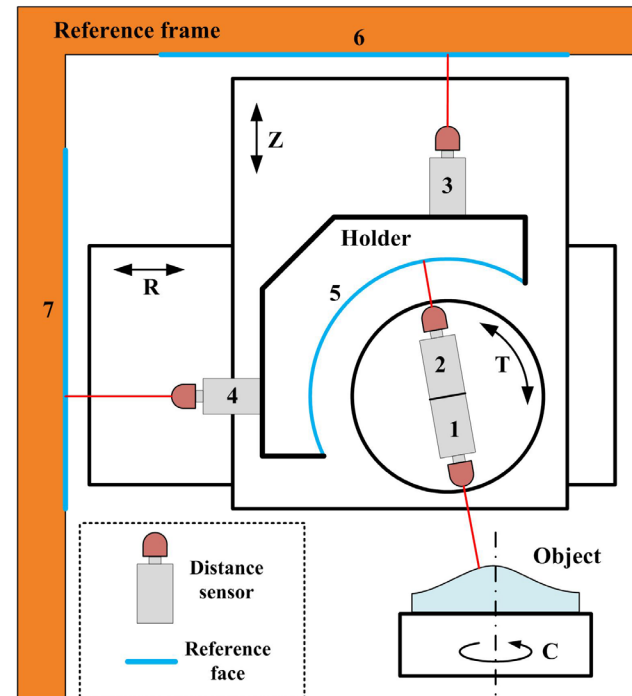


**Figure 19.** MWI-based 3D profilometer for freeform surfaces.

to the reference faces 6, 7 can be determined by means of the further distance sensors 3 and 4. Other point-wise measuring methods for on-line inspection based on low-coherence interferometry are being investigated as well [228].

**4.2.2. Point-wise wavelength scanning.** Improvement of the point scanning setup may rely on the tunable light source in order to sweep the light beam with different wavelengths across the measured surface to take a line profile of the height variation [229]. This method is similar to the dispersive interferometer mentioned in section 3.2.2 where a blazed grating is adopted to angularly disperse an incident light beam which is then collimated onto the object. Figure 20 illustrates a schematic of the wavelength scanning probe and the angle sign definition for gratings. The zero-order diffracted light that is used in the reference arm is the special case of the grating

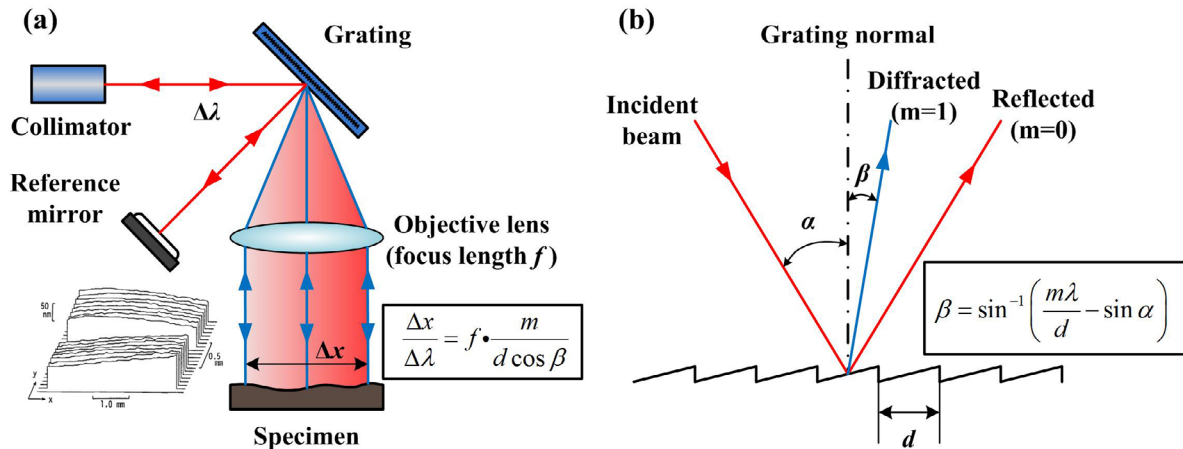


**Figure 20.** Wavelength scanning profilometer using a grating. (a) Optical probe schematic. (b) Angle sign definition for gratings.

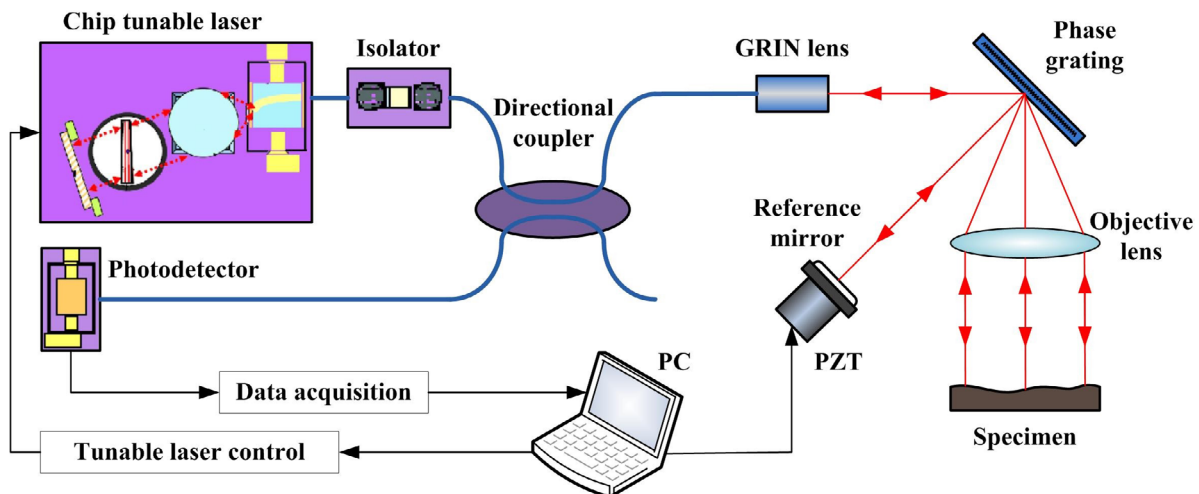


**Figure 21.** Configuration of the integrated interferometric system based on chip-level tunable laser.

equation (when  $m = 0$ ). This brings convenience to the measurement as the wavelength is swept and the first order beam ( $m = 1$ ) moves across the object surface, while the reference beam remains stationary [230].

In terms of the lateral measuring range, it is convenient to change the scan width  $\Delta x$  in two ways: adjusting the incident angle  $\alpha$  or varying the effective focal length  $f$ . Obviously the focal length is fixed for a given optical probe as the lens must be physically changed, and varying the incident angle may only be done over a short range before the onset of non-linearity in the scan. For the 3D profilometry, by moving the specimen in the horizontal direction, the surface profile can be obtained.

In order to further enhance the flexibility and realize online measurements, chip-level interferometers that integrate various components of the interferometric sensor system onto a single optical chip are becoming more attractive [231, 232]. The chip-level interferometers are not only insensitive to electromagnetic noise, suitable for applications in a harsh environment, but also have the advantages of high integration, better reliability, ability for mass production, and low cost [233]. An integrated optical coupler and a chip tunable laser were successfully used in fiber optic interferometric systems

for on-line surface measurements [234, 235]. The configuration of the system is shown in figure 21, the chip tunable laser together with the fiber components including an optical fiber isolator, a directional fiber coupler and a photodetector is combined to build an integrated interferometric system.

**4.2.3. Spectrally resolved WLI.** Point-wise profilometry seems to lack speed, while spectrally resolved white light interferometry (SRWLI) can quickly provide a 2D line profile of the object [236]. As shown in figure 22(a), the entrance slit (ES) selects a line from the white light interferogram for profilometry, and then it is spectrally decomposed using a spectrometer to generate a set of monochromatic interferograms which encode the phase as a function of wavenumber. The interferogram displayed at the exit plane of the spectrometer has a continuous variation of wavelength along the chromaticity axis. The OPD can be calculated as the slope of the phase versus wavenumber linear fit. Many techniques such as Fourier transform [225], spatial phase shifting [237], temporal phase shifting [238], Hilbert transform [239], windowed Fourier transform [240] and wavelet transform [241] have been put forward to determine the phase in the spectral domain. The temporal phase-shifting technique offers

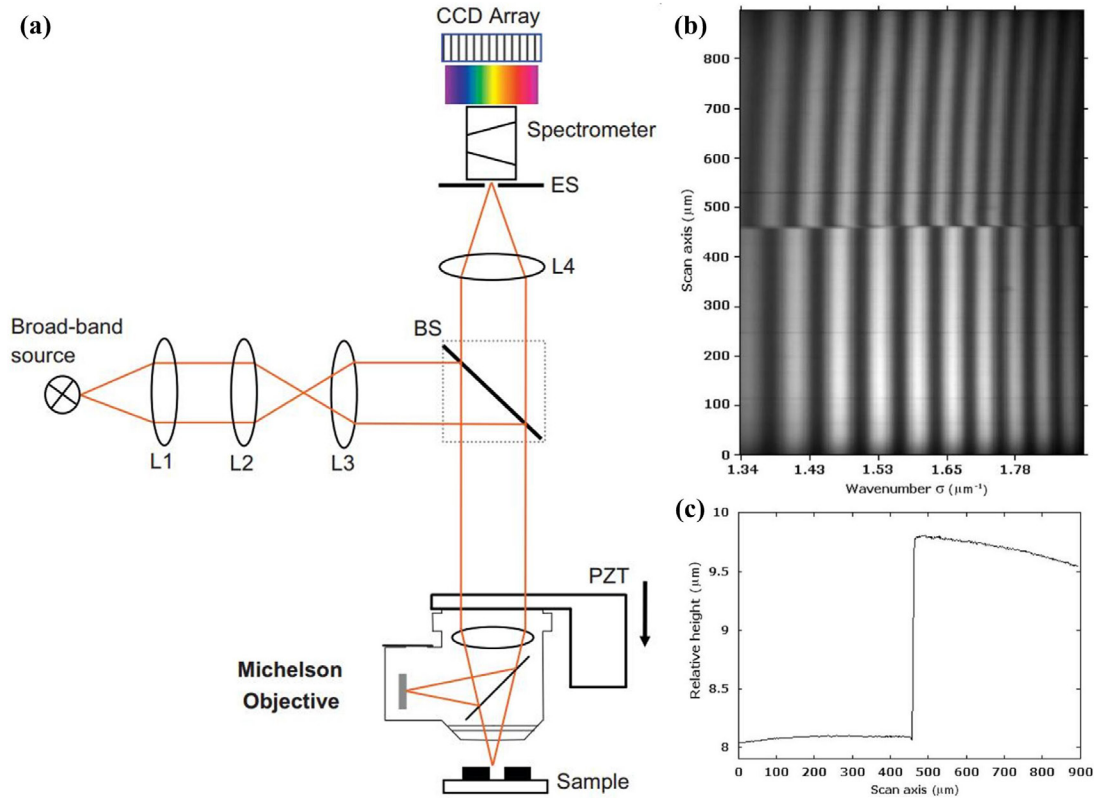


**Figure 22.** SRWLI for line profile measurement. (a) Setup. (b) Spectral interferogram of a specimen with a step. (c) Measurement result. Reprinted from [245], Copyright 2009, with permission from Elsevier.

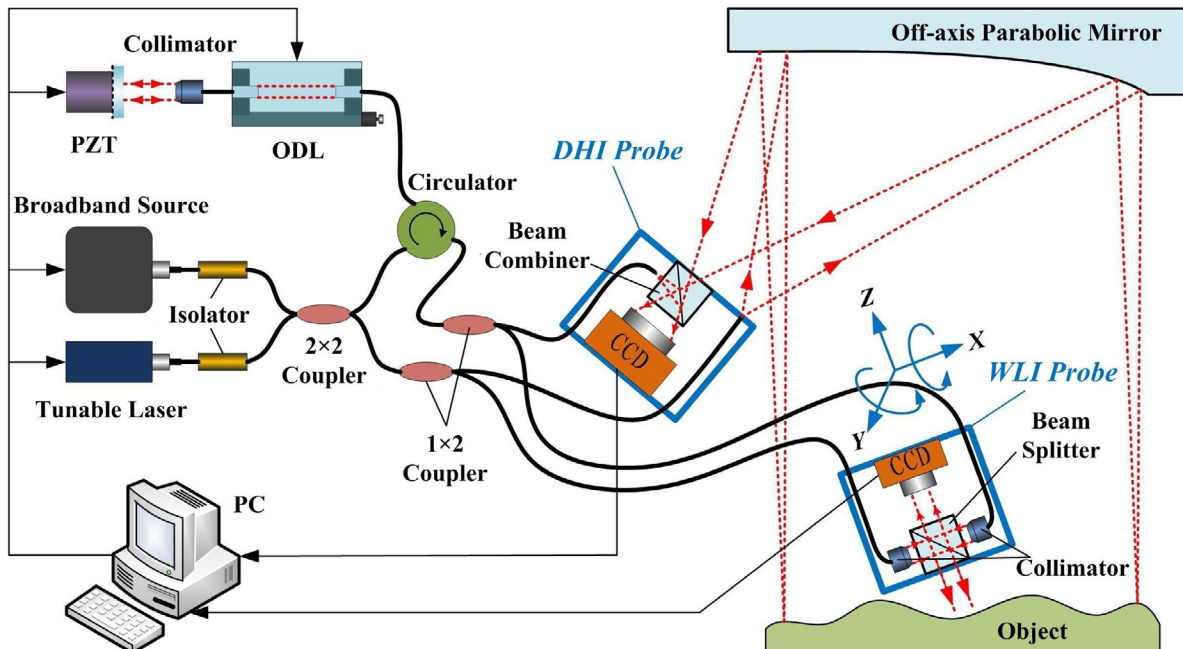


**Figure 23.** A complementary integration of the large-aperture DHI and the sub-aperture stitching WLI. ODL, optical delay line.

accurate results but needs several phase-shifted frames. The Fourier transform, spatial phase shifting, Hilbert transform, windowed Fourier transform and wavelet transform methods only need one spectrally resolved interferogram and are more attractive. Debnath *et al* [242] made a comparative study of these techniques, as illustrated in figure 22, where (b) shows

the spectral interferogram of a specimen with a step and (c) is the measurement result by the Hilbert transform method.

**4.2.4. Sub-aperture stitching interferometry.** As an alternative to large-aperture interferometry, full-field interferometers are combined with scanning and positioning devices in

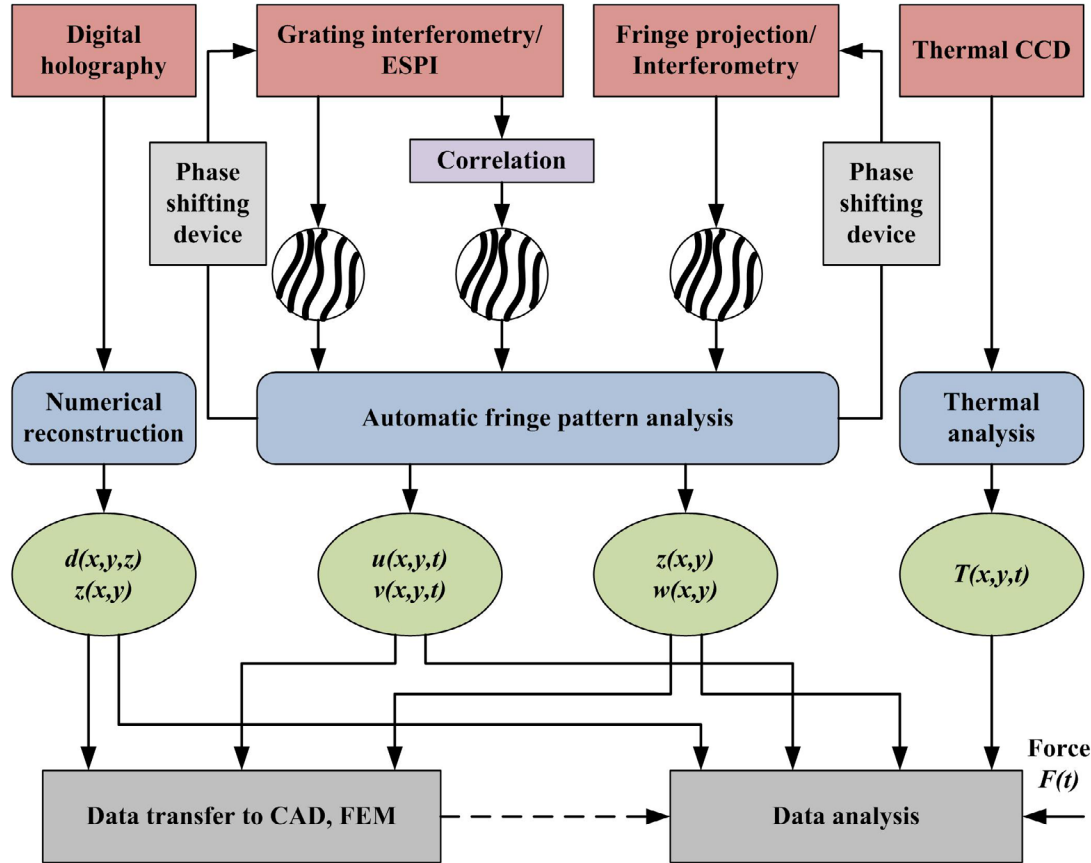


**Figure 24.** The concept of micromeasurement station. Reprinted from [254], Copyright 2002, with permission from Elsevier.

order to obtain the whole geometry of a macroscopic object with high lateral resolution. This method depends on the sub-aperture stitching technique [243] and needs the object to be adjusted to different positions to make sure the sub-apertures overlap appropriately. PSI is a commonly adopted method to measure the surface information on each sub-aperture. However, it may result in additional measurement uncertainty with large numbers of sub-apertures. To achieve trans-scale measurement with low uncertainty, we designed a complementary integrated system that combines the large-aperture DHI and the sub-aperture stitching WLI. As shown in figure 23, the DHI subsystem is used to complete a rough measurement of the overall profile of the object, and thus establish a reasonable way of path planning, and then guide the WLI probe to measure the local detail features with nanometer accuracy.

As the PSI method may be time consuming on data acquisition, capturing four  $\pi/2$  phase-shifted sub-aperture images in a single shot is possible by using the pixelated phase mask technique [244]. Rotational symmetric aspherical objects can be tested by shifting a Fizeau interferometer in well-known steps to different positions along the optical axis and using PSI at each position [245]. This generates a set of circular surface sections where the tested surface locally fits the spherical wavefront. Another appealing method is the tilted wave interferometry which illuminates the object with a series of tilted wavefronts [246, 247]. This is similar to sub-aperture stitching but it works without mechanical scanning.

## 5. Flexible measurement methods

Since the demands of the complexity and accuracy of dimensional and surface metrology are ever-growing, multi-sensor data fusion methods are proposed to obtain holistic information and improve the reliability or reduce the uncertainty of measurement data [248]. Flexible measurement is a synergistic application of various sensors to carry out a given task under complicated working conditions. Durrant-Whyte [249] classifies these multi-sensor integrated systems into complementary, competitive and cooperative integration, according to their sensor configurations.

### 5.1. Complementary integration

In a complementary system, sensors do not directly relate to each other, but can be combined to obtain a variety of information and show multifunctional measurement ability. For instance, we propose to develop a fully parametric detection system for grinding optical surfaces. WLI is used to obtain the surface topography and roughness, and furthermore, a confocal microscope is adopted for tomography of the subsurface damage depth. Blain *et al* [250] combined shearography and interferometric fringe projection in a single device, which can measure both microdeformations and the 3D shape of a surface. The Institute of Micromechanics and Photonics of Warsaw University of Technology [251] proposed the concept

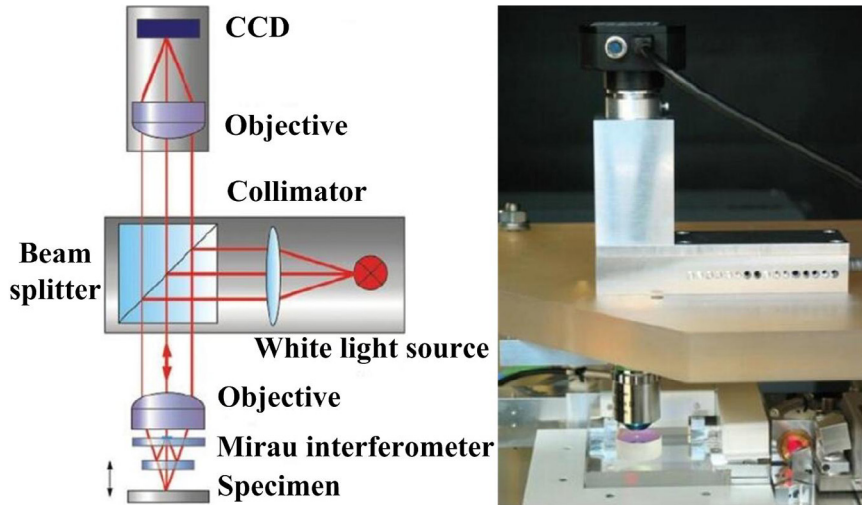


**Figure 25.** WLI microscope integrated with the NPM machine. Reproduced from [259]. © IOP Publishing Ltd. All rights reserved.

of an integrated measurement station, as shown in figure 24. Interferometry, fringe projection PMP, electronic speckle pattern interferometry (ESPI), digital holography, grating interferometry and thermovision units are specially designed and properly arranged at an optical table for integration measurements. Details about optical, mechanical, and electro-optical design for massive parallel inspection were introduced in [252].

In the same way, a 3D nanopositioning and nanomeasuring machine (NPM-machine) [253], developed by the Institute of Process Measurement and Sensor Technology of the Technical University Ilmenau, can be available for various tasks such as large-area scanning probe microscopy, mask and wafer inspection, as well as mechanical precision workpieces measurement by combining with different types of sensing probe (scanning probe, interference microscope, focusing probe). The challenge in these complementary systems is the selection of the best sensor chain for each individual inspection step. It needs a good knowledge about the performance of each sensor. Software and hardware assistants for optical measurement systems which are integrated with precision multi-axis actuators have to be designed to efficiently make an optimal selection of the appropriate sensor with respect to the required resolution, measurement uncertainty, range and processing time [254].

### 5.2. Competitive integration

A multi-sensor integrated configuration is competitive if each sensor performs an independent measurement of the same property to get reliable, holistic information. For example, a hybrid AFM measurement system which has been combined with VSWLI is developed by Guo *et al* [255]. In this method, the sample is measured first by VSWLI to obtain an overall coarse topography, and further measurement is carried out with higher resolution by AFM. Such competitive integrations are adopted to reduce the measurement uncertainty and to avoid erroneous measurements. Another illustration is

shown in figure 25; if a WLI microscope is integrated into NPM machines [256], the measuring range will extend up to 5 mm, and that means the requirements of both high measurement resolution and relatively large measuring range are met simultaneously. A multifunctional nanoanalytics and long-range SPM using the NPM machine was reported [257], and a high precision measurement with nanometer uncertainty over a range of 25 mm × 25 mm × 5 mm was realized.

Basile *et al* [91] combined the XRI with a laser interferometer to enlarge the measuring range so that the measurement uncertainty of 10 pm can be realized in the measuring range of  $\pm 1$  mm. Yacoot *et al* [37] investigated the potential combination of an x-ray interferometer and optical interferometer as a 1D long-range, high-resolution scanning stage for an AFM in order to measure variations in the grating period. Park *et al* [258] developed a 2D combined optical and x-ray interferometer, which combines an x-ray interferometer, two optical interferometers and an AFM. Research and applications of these competitive integrated flexible measurement systems are constantly improved [259–262].

### 5.3. Cooperative integration

A cooperative integrated configuration makes use of the mutual enhancing sensors to obtain information that cannot be directly obtained by the sensors independently. A typical illustration of this cooperation is the coordinate measuring machine (CMM) based system which comprises an integrating visual sensor and an optical probe. Initially, the visual sensor is used to find the location to be measured, and then the CMM, as the carrier of the optical probe, measures the location. Finally the measurements are carried out by the high precision optical probe. In order to improve the existing comparative procedure for measuring complex dimensions and surfaces, Tasic *et al* [263] developed a measurement system which consists of a CMM and a laser interferometer for traceable absolute measurements. The laser interferometer is used for traceable measurement, and the CMM is only adopted as

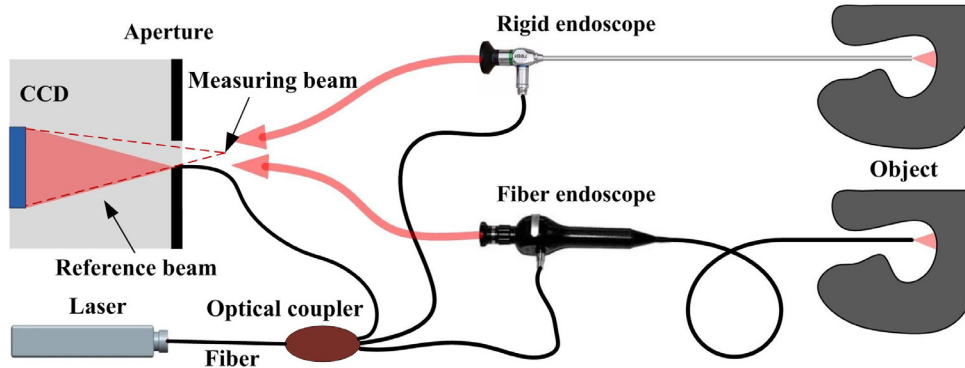


**Figure 26.** Setup with rigid and flexible fiber endoscope for investigations using digital holographic interferometry.

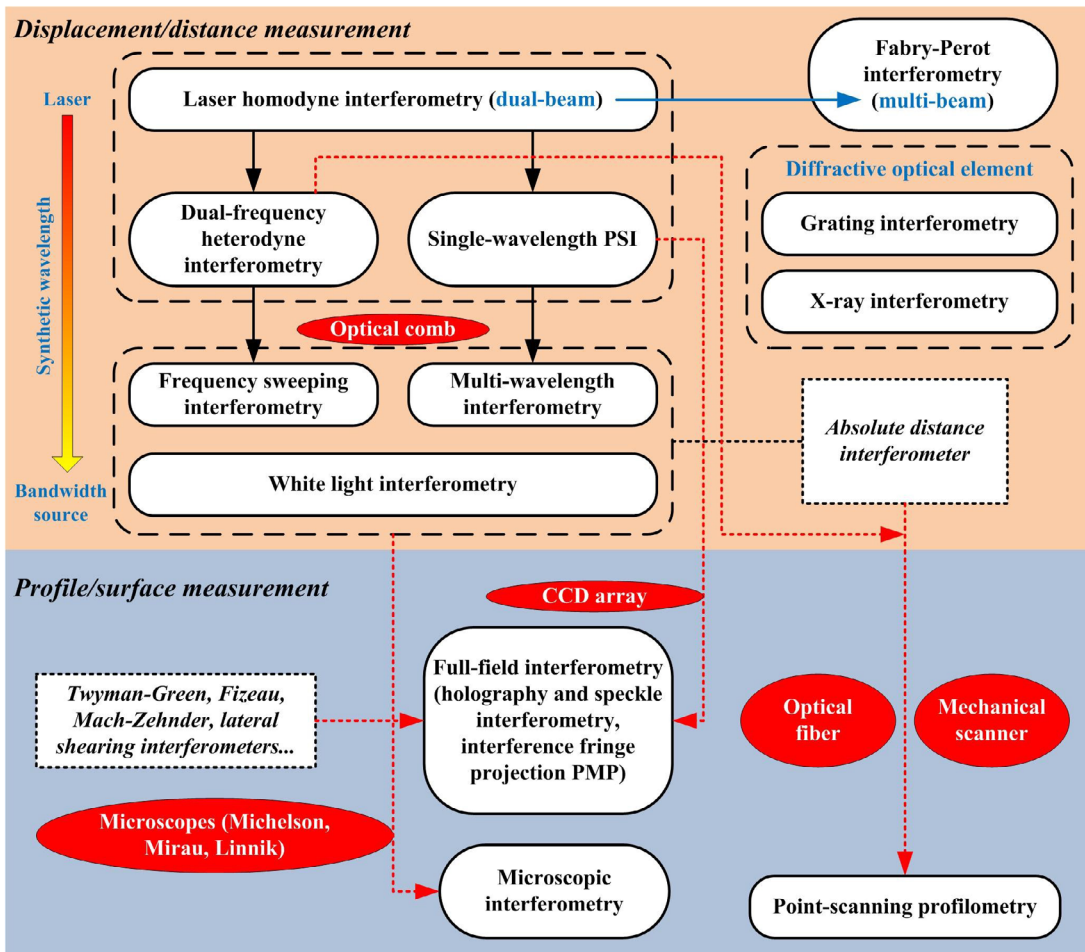


**Figure 27.** Classification of the existing interferometric techniques.

a guiding mechanism for the probe. Coordinate measurement systems combined with different optical sensors have been discussed by Ettemeyer [264].

To further enhance the flexibility and make the measurement of hidden structures possible, the combination of optical metrology and endoscopy was introduced [265, 266]. Gao *et al* [267] proposed a phase-shifting endoscopic ESPI system for the measurement of cavities with a small access aperture. A combination of a pulsed holographic interferometric system and endoscopes was reported [18], and the adoption of optical fibers makes it more flexible so that it can be applied under industrial operations and harsh environments, as shown

in figure 26. Another practical application is the endoscopic fringe projection profilometry [268], and it showed tremendous potential with the development of multicore optical fibers [269].

## 6. Discussions and remarks

### 6.1. Analysis and summary

State-of-the-art geometric measurement techniques based on interferometry can be classified in different ways. Figure 27 shows a development chart of the interferometric techniques

mentioned in this paper. For different measurement requirements, they can be divided into single-point interferometry for displacement and distance measurement, and point-scanning profilometry and full-field interferometry for surface characterization. They can also be classified by the types of optical configurations adopted in the measurement systems, for instance, Michelson, Fabry–Perot, Twyman–Green, Fizeau, Mach–Zehnder and even common path configurations such as point diffraction and lateral shearing interferometers. According to the beamsplitter or the measurement benchmark, there are grating interferometry and x-ray interferometry. In terms of the light source, they can be classified by the number of wavelengths, such as single wavelength interferometry, multi-wavelength interferometry, frequency sweeping interferometry, white light interferometry.

Considering the measurement requirements and the different applications, table 1 shows the performances, merits and limitations in various types of interferometric methods. For example, although point-wise interferometry seems time-consuming, it is a feasible technique for the complex aspheric or freeform surfaces that are not easily adapted in full-field interferometry.

## 6.2. Measurement resolution, range and 5D metrology

**6.2.1. Contradiction between high resolution and large range.** As a means of establishing traceability, optical interferometric technology has encountered a common problem in that the accuracy of SPM is at least an order of magnitude higher than that of the existing interferometer, which means the existing measurement instruments do not meet the requirements of the actual calibration. Multireflection interferometric methods have a theoretical resolution of up to subpicometer resolution, but its application is still limited because of the complexity of the interferometer structure, the strictness of manufacturing requirements, the difficulty of adjustments, how easily it is affected by the environment and the need for excellent monochromatic laser light source. In figure 28 we present a diagram illustrating the applicable measurement resolution and working range of the displacement and distance measuring techniques discussed. WLI theoretically has no range limit for absolute distance measurement but suffers from mechanical scanning error which leads to a low resolution. X-ray interferometry can perform sub-*pm* resolution measurement while its measuring range is  $\sim 10 \mu\text{m}$ . Combining several interferometric techniques to make up for their own shortcomings is a breakthrough in solving the contradiction between high resolution and large range.

**6.2.2. Lateral resolution enhancement (*x-y*).** Interferometric microscopes provide a fast, non-contact method for mapping surface microstructure in 2D or 3D with excellent vertical resolution. Subnanometer vertical resolution can be realized by selecting the proper algorithms. According to the theory of diffraction resolution limit proposed by Abbe in 1883, however, the lateral resolution is limited by the optical resolution, as with any optical microscope. Current methods for

improving the lateral resolution mainly include: using a very short wavelength of radiation such as UV, x-ray and electron; improving the refractive index or the NA of the microscope such as the adoption of oil immersed objective. In addition to the method for replacing photons with electrons that will significantly improve the resolution, the other solutions can only slightly improve the resolution. The conventional optical microscope based on the diffraction effect cannot meet the requirements of tens of nanometers. The super-resolution method will be an important research topic in the future.

**6.2.3. 5D optical metrology (*x-y-z-t-λ*).** An eternal subject of scientific exploration in the microscopic world is undoubtedly the pursuit for resolution which includes spatial resolution (*x-y-z*), temporal resolution (*t*) and spectral resolution ( $\lambda$ ), especially corresponding to 3D spatial measurement, 4D (*x-y-z-t*) spatial-temporal measurement and 5D (*x-y-z-t-λ*) spatial-temporal-spectral measurement using the super-continuum white light laser. Spatial resolution represents the detailed features of a 3D object, while temporal resolution characterizes the dynamic evolution. The spectral imaging can be used to analyze the interactions of different wavelengths and objects, study the composition, material properties etc. Further development of interferometric microscopy will be 4D and 5D interferometry.

## 6.3. Flexible measurement instrument

**6.3.1. High integration.** Flexible measurement capability is achieved by combining one or more measurement methods and techniques to overcome the constraints and limitations of a single method, so as to achieve a flexible, intelligent real-time measurement. To get more complete information, firstly we should consider the performances of each instrument applied in the integrated system. Further research into interferometric systems will focus on the multi-sensor integrated flexible measurement method which runs in an unknown and dynamic environment. The development of chip-level interferometric microsensor and fiber optic sensing technology will mean the level of integration is increased substantially. It is compact and robust as environmental noise and disturbance can be eliminated, and suitable for on-line application. In data fusion, artificial intelligence and neural networks will continue to be an important topic.

**6.3.2. High intelligence.** With the development of industrial technology, it is required that the measuring instrument is capable of making a highly intelligent analysis of the measured object, so as to automatically select the optimal measurement method. Most of the current integrated measurement instruments are neither systematic nor intelligent. The idea of intelligent measurement is to choose the optimal combination of sensors according to the measured object and parameters, and it can be divided into the pre- and real-time selection method. The former makes the optimal allocation of sensors in advance, and the latter can be configured to achieve a local optimum with environment changes.

**Table 1.** Comparison of interferometric methods.

Items	Methods	Performances	Merits	Limitations
Displacement measurement	Homodyne interferometry	0.1 nm resolution with meters range. Speed: $1 \text{ m s}^{-1}$	Simplest configuration; low cost	DC offset error; sensitive to environmental disturbances; periodic nonlinearity
	Heterodyne interferometry	0.1 nm resolution with meters range Speed: $1 \text{ m s}^{-1}$ (4 MHz of Zeeman); $5.1 \text{ m s}^{-1}$ (20 MHz of AOM)	Low noise, strong anti-interference ability	Periodic nonlinearity, mode coupling error
	Fabry–Perot interferometry	0.001 nm resolution with micrometers range, which depends on the beat frequency. Speed: $10 \text{ nm s}^{-1}$	Common light path, insensitive to environmental disturbances	Difficult optical alignments, limited measuring range, strict requirement for source monochromaticity
	X-ray interferometry	0.005 nm resolution with $\sim 10 \mu\text{m}$ range, which is limited by the size of crystal. Speed: $10 \mu\text{m s}^{-1}$	High resolution, high accuracy	Low measuring speed, small range, difficult to machine the single crystal silicon
	Grating interferometry	Resolution: 1–10 nm. Accuracy: $0.1 \mu\text{m}/100 \text{ mm}$ . Range: $\sim 200 \text{ mm}$ . Speed: $100 \text{ mm s}^{-1}$	Use grating constant as benchmark, rarely affected by source variations, large range	Low accuracy, precision grating lithography difficulty
Distance measurement	Frequency sweeping interferometry	Nanometer resolution with a nonambiguous range of millimeters (depends on $\Delta v$ )	High accuracy could remain in large range	High demand for light source, limited speed for frequency sweeping
	MWI	Nanometer resolution, range of $\lambda_s/4$ ( $\lambda_s$ refers to the synthetic wavelength)	Large range, no need for fringe counting	Large synthetic wavelength leads to relatively low accuracy
	WLI	Micrometer resolution, range depends on the travel distance of the scanning mechanism	Low demand for light source, no limit for measuring range	Low accuracy, complex demodulation algorithm, vibration of scanning mechanism
Profile and surface measurement	Single-point scanning profilometry (MWI based absolute distance measurement)	Nanometer vertical resolution, lateral resolution and range depend on the multidimensional scanning mechanism	High flexibility for surfaces with large variations such as aspherics (hundreds millimeter achievable)	Low measuring speed, sparse sampling points
	Full-field monochromatic PSI	Subnanometer vertical resolution, horizontal resolution and range depend on the size of the pixel and the magnification of the objective lens	High accuracy for slowly varying, smooth surface	$\lambda/2$ height ambiguity, limited horizontal resolution and range
	Full-field VSWLI		No height ambiguity, available for discontinuities, steps and high roughness	Relatively low accuracy, limited horizontal resolution and range

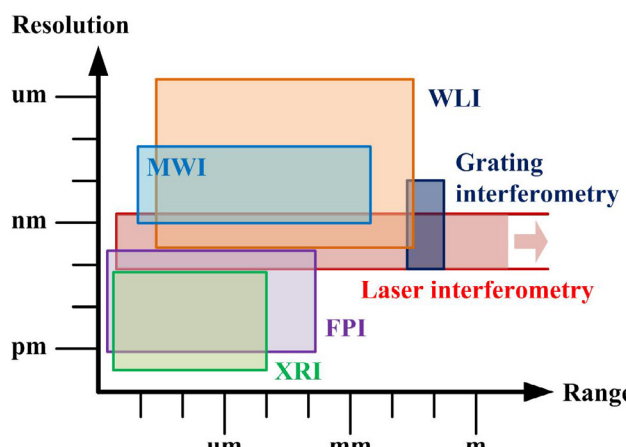


**Figure 28.** Comparison of typical resolution and working range of the interferometric techniques discussed in this paper.

## 7. Conclusions

We have witnessed major advances in interferometry in the last century. While several new breakthroughs were explored earlier, the revolution that triggered the major prosperity of interest was doubtless the introduction of lasers, which have broken through most of the measurement limitations caused by thermal sources. This has lead to high-performance laser interferometers, such as the heterodyne interferometer, the Fabry–Perot interferometer, and the self-mixing interferometer. To overcome the phase ambiguity and realize absolute distance measurement, MWI techniques have been developed to greatly extend the measuring range to meet the requirements for large scale objects. Another contribution was the ever-growing adoptions of detector arrays to substitute for conventional methods of recording and analyzing interferograms. Monochromatic phase-shifting techniques, multi-wavelength methods and white light interference were then progressively introduced in interferometry. With the development of high precision DOE, new principles and methods, such as grating interferometry and x-ray interferometry, have provided a new perspective for interferometry. New applications have arisen from the adoption of optical fibers and chip-level components to develop the analogues of traditional interferometers, which have the advantages of high integration, and low noise levels, and can be used to achieve extremely high sensitivity. Interferogram projection PMP has also been widely researched in academia and applied in industrial fields because of the advantages of full-field acquisition, fast data processing and availability for diffuse objects. For micro-surface metrology, microscopic interferometry has become a standard metrological method in ultra-precision manufacturing processes and has formed a great many complete sets of measuring instruments with a high level of automation. An eternal subject of scientific exploration in the microscopic world is undoubtedly the pursuit for resolution, and a further development will unfold in 4D spatial-temporal measurement and 5D spatial-temporal-spectral measurement.

Multi-sensor integrated flexible measurement methods have been proposed to perform versatile measurements with

holistic, more accurate and reliable information. Most of the proposed methods are not intelligent or highly integrated, but represent rather specific solutions for given measurement tasks. Therefore, flexible measurement will continue to be very innovative and interesting in the future as it encompasses more areas of dimensional and surface metrology.

## Acknowledgment

The authors are grateful for the support of National Science Fund for Excellent Young Scholars (No. 51722509), National Natural Science Foundation of China (No. 51575440), National Key R&D Program of China (2017YFB1104700) and Shaanxi Science and Technology Project (No. 2016GY-011).

## ORCID iDs

Shuming Yang  <https://orcid.org/0000-0002-8957-8751>

## References

- [1] Dai G, Pohlenz F, Xu M, Koenders L, Danzebrink H U and Wilkening G 2006 Accurate and traceable measurement of nano- and microstructures *Meas. Sci. Technol.* **17** 545–52
- [2] Chugui Y, Verkhoglyad A, Poleschuk A, Korolkov V, Sysoev E and Zavyalov P 2013 3D optical measuring systems and laser technologies for scientific and industrial applications *Meas. Sci. Rev.* **13** 322–8
- [3] Vorburger T V, Rhee H G, Renegar T B, Song J F and Zheng A 2007 Comparison of optical and stylus methods for measurement of surface texture *Int. J. Adv. Manuf. Technol.* **33** 110–8
- [4] Vilaça J L, Fonseca J C and Pinho A M 2010 Non-contact 3D acquisition system based on stereo vision and laser triangulation *Mach. Vis. Appl.* **21** 341–50
- [5] Chen L C and Huang C C 2005 Miniaturized 3D surface profilometer using digital fringe projection *Meas. Sci. Technol.* **16** 1061–8
- [6] Liu X M, Yu W U, Zhang P F and Yang G G 2006 Research of a nanometer system for displacement measurement based on optical lever *J. Optoelectron. Laser* **17** 969–73
- [7] Yin Y, Wang M, Gao B Z, Liu X and Peng X 2015 Fringe projection 3D microscopy with the general imaging model *Opt. Express* **23** 6846–57
- [8] Marin V E, Kashino Z, Chang W H W, Luitjens P and Nejat G 2017 Design of three-dimensional structured-light sensory systems for microscale measurements *Opt. Eng.* **56** 124109
- [9] Hamilton D K and Wilson T 1982 Three-dimensional surface measurement using the confocal scanning microscope *Appl. Phys. B* **27** 211–3
- [10] Chun B S, Kim K and Gweon D 2009 Three-dimensional surface profile measurement using a beam scanning chromatic confocal microscope *Rev. Sci. Instrum.* **80** 073706
- [11] de Groot P, Biegen J, Clark J, de Lega X C and Grigg D 2002 Optical interferometry for measurement of the geometric dimensions of industrial parts *Appl. Opt.* **41** 3853–60
- [12] Shafir E and Berkovic G 2012 Optical methods for distance and displacement measurements *Adv. Opt. Photonics* **4** 441–71
- [13] Petley B W 1983 New definition of the metre *Nature* **303** 373–6

- [14] Felder R 2005 Practical realization of the definition of the metre, including recommended radiations of other optical frequency standards (2003) *Metrologia* **42** 323–5
- [15] Peggs G N and Yacoot A 2002 A review of recent work in sub-nanometre displacement measurement using optical and x-ray interferometry *Phil. Trans. R. Soc. A* **360** 953–68
- [16] Goodwin E P and Wyant J C 2006 *Field Guide to Interferometric Optical Testing* (Bellingham, WA: SPIE Press)
- [17] Wang Y, Xie F, Ma S and Dong L 2017 Review of surface profile measurement techniques based on optical interferometry *Opt. Lasers Eng.* **93** 164–70
- [18] Tiziani H J and Pedrini G 2013 From speckle pattern photography to digital holographic interferometry *Appl. Opt.* **52** 30–44
- [19] Schnars U and Jüptner W P 1994 Digital recording and reconstruction of holograms in hologram interferometry and shearography *Appl. Opt.* **33** 4373–7
- [20] Lee B H, Kim Y H, Park K S, Eom J B, Kim M J, Rho B S and Choi H Y 2012 Interferometric fiber optic sensors *Sensors* **12** 2467–86
- [21] Dorriño B V and Fernández J L 1999 Phase-evaluation methods in whole-field optical measurement techniques *Meas. Sci. Technol.* **10** R33
- [22] BIPM, IEC, IFCC, ILAC, IUPAC, IUPAP, ISO and OIML 2008 *International Vocabulary of Metrology—Basic and General Concepts and Associated Terms (VIM)* 3rd edn (Paris: JCGM) ([https://www.bipm.org/utils/common/documents/jcgm/JCGM\\_200\\_2012.pdf](https://www.bipm.org/utils/common/documents/jcgm/JCGM_200_2012.pdf))
- [23] Michelson A A and Benoit J R 1895 *Trav. Mem. Bur. Int. Poids Mes.* **11** 1
- [24] Helmcke J 2003 Realization of the metre by frequency-stabilized lasers *Meas. Sci. Technol.* **14** 1187–99
- [25] Rerucha S, Yacoot A, Pham T M, Cizek M, Hucl V, Lazar J and Cip O 2017 Laser source for dimensional metrology: investigation of an iodine stabilized system based on narrow linewidth 633 nm DBR diode *Meas. Sci. Technol.* **28** 045204
- [26] ISO3650 1999 *Geometrical Product Specifications—Length Standards—Gauge Blocks* (Geneva: International Standards Organization)
- [27] Misumi I, Gonda S, Huang Q, Keem T, Kurosawa T and Fujii A 2005 Sub-hundred nanometre pitch measurements using an afm with differential laser interferometers for designing usable lateral scales *Meas. Sci. Technol.* **16** 2080–90
- [28] Quinn T J 2003 Practical realization of the definition of the metre, including recommended radiations of other optical frequency standards *Metrologia* **40** 103–33
- [29] Jones D J, Diddams S A, Ranka J K, Stentz A, Windeler R S, Hall J L and Cundiff S T 2000 Carrier-envelope phase control of femtosecond mode-locked lasers and direct optical frequency synthesis *Science* **288** 635–9
- [30] Quenelle R C 1983 Nonlinearity in interferometer measurements *Hewlett-Packard J.* **34** 10
- [31] Sutton C M 1987 Nonlinearity in length measurements using heterodyne laser Michelson interferometry *J. Phys. E: Sci. Instrum.* **20** 1290–2
- [32] Wu C and Su C 1996 Nonlinearity in measurements of length by optical interferometry *Meas. Sci. Technol.* **7** 62–8
- [33] Ellis J D, Baas M, Joo K N and Spronck J W 2012 Theoretical analysis of errors in correction algorithms for periodic nonlinearity in displacement measuring interferometers *Precis. Eng.* **36** 261–9
- [34] Cosijns S J A G, Haitjema H and Schellekens P H J 2002 Modeling and verifying non-linearities in heterodyne displacement interferometry *Precis. Eng.* **26** 448–55
- [35] Howard L, Stone J and Fu J 2001 Real-time displacement measurements with a Fabry–Perot cavity and a diode laser *Precis. Eng.* **25** 321–35
- [36] Martin J, Kuetgens U, Stumpel J and Becker P 1998 The silicon lattice parameter—an invariant quantity of nature *Metrologia* **35** 811–7
- [37] Yacoot A and Koenders L 2003 From nanometre to millimetre: a feasibility study of the combination of scanning probe microscopy and combined optical and x-ray interferometry *Meas. Sci. Technol.* **14** N59–63
- [38] Evans C J and Bryan J B 1993 Compensation for errors introduced by nonzero fringe densities in phase-measuring interferometers *CIRP Ann.-Manuf. Technol.* **42** 577–80
- [39] Schulz M, Blobel G, Fortmeier I, Stavridis M and Elster C 2015 Traceability in interferometric form metrology *Proc. SPIE* **9525** 95251F
- [40] Haitjema H 2008 Achieving traceability and sub-nanometer uncertainty using interferometric techniques *Meas. Sci. Technol.* **19** 084002
- [41] Evans C J and Kestner R N 1996 Test optics error removal *Appl. Opt.* **35** 1015–21
- [42] Malacara Z, Servin M and Malacara Z 2016 *Interferogram Analysis for Optical Testing* (Boca Raton, FL: CRC Press)
- [43] Chen L C, Nguyen D T and Chang Y W 2016 Precise optical surface profilometry using innovative chromatic differential confocal microscopy *Opt. Lett.* **41** 5660–3
- [44] Decker J E and Pekelsky J R 1997 Uncertainty evaluation for the measurement of gauge blocks by optical interferometry *Metrologia* **34** 479–93
- [45] Lewis A 1994 Measurement of length, surface form and thermal expansion coefficient of length bars up to 1.5 m using multiple-wavelength phase-stepping interferometry *Meas. Sci. Technol.* **5** 694–703
- [46] O'Hora M, Bowe B and Toal V 2006 Phase-stepped gauge block interferometry using a frequency-tunable visible laser diode *Appl. Opt.* **45** 5607–13
- [47] Dorriño B V and Outumuro I 2013 Design of an interferometric system for gauge block calibration *Opt. Eng.* **52** 045601
- [48] Matus M, Haas S, Piree H, Gavalyugov V, Tamakyarska D and Thalmann R 2016 Measurement of gauge blocks by interferometry *Metrologia* **53** 04003
- [49] Haitjema H and Kotte G 1998 Long gauge block measurements based on a Twyman-Green interferometer and three stabilized lasers *Proc. SPIE* **3477** 25–34
- [50] Kuriyama Y, Yokoyama Y, Ishii Y, Ishikawa J and Makino H 2006 Development of a new interferometric measurement system for determining the main characteristics of gauge blocks *CIRP Ann.-Manuf. Technol.* **55** 563–6
- [51] Bobroff N 1993 Recent advances in displacement measuring interferometry *Meas. Sci. Technol.* **4** 907–26
- [52] Kim J A, Kim J W, Kang C S, Eom T B and Ahn J 2008 A digital signal processing module for real-time compensation of nonlinearity in a homodyne interferometer using a field-programmable gate array *Meas. Sci. Technol.* **20** 017003
- [53] Hu P, Zhu J, Zhai X and Tan J 2015 DC-offset-free homodyne interferometer and its nonlinearity compensation *Opt. Express* **23** 8399–408
- [54] Hu P, Zhu J, Guo X and Tan J 2015 Compensation for the variable cyclic error in homodyne laser interferometers *Sensors* **15** 3090–106
- [55] Yan L, Chen B and Wang B 2017 A differential Michelson interferometer with orthogonal single frequency laser for nanometer displacement measurement *Meas. Sci. Technol.* **28** 045001
- [56] Požar T, Gregorčič P and Možina J 2011 A precise and wide-dynamic-range displacement-measuring homodyne quadrature laser interferometer *Appl. Phys. B* **105** 575–82
- [57] Cui J, He Z, Jiu Y, Tan J and Sun T 2016 Homodyne laser interferometer involving minimal quadrature phase error to obtain subnanometer nonlinearity *Appl. Opt.* **55** 7086–92
- [58] Pisani M 2009 A homodyne Michelson interferometer with sub-picometer resolution *Meas. Sci. Technol.* **20** 084008

- [59] Cheng Z, Gao H, Zhang Z, Huang H and Zhu J 2006 Study of a dual-frequency laser interferometer with unique optical subdivision techniques *Appl. Opt.* **45** 2246–50
- [60] Kochert P, Flugge J, Weichert C, Koning R and Manske E 2012 Phase measurement of various commercial heterodyne He-Ne laser interferometers with stability in the picometer regime *Meas. Sci. Technol.* **23** 074005
- [61] Yu H, Liu H, Li X, Ye G, Shi Y, Yin L and Jiang W 2015 Calibration of non-contact incremental linear encoders using a macro–micro dual-drive high-precision comparator *Meas. Sci. Technol.* **26** 095103
- [62] Choi H, Park K and La J 2005 Novel phase measurement technique of the heterodyne laser interferometer *Rev. Sci. Instrum.* **76** 093105
- [63] Park Y and Cho K 2011 Heterodyne interferometer scheme using a double pass in an acousto-optic modulator *Opt. Lett.* **36** 331–3
- [64] Kimachi A 2007 Real-time heterodyne imaging interferometry: focal-plane amplitude and phase demodulation using a three-phase correlation image sensor *Appl. Opt.* **46** 87–94
- [65] Meskers A J, Spronck J W and Schmidt R H 2014 Heterodyne displacement interferometer, insensitive for input polarization *Opt. Lett.* **39** 1949–52
- [66] Demarest F C 1999 High-resolution, high-speed, low data age uncertainty, heterodyne displacement measuring interferometer electronics *Meas. Sci. Technol.* **9** 1024–30
- [67] Eom T, Choi T, Lee K, Choi H and Lee S 2002 A simple method for the compensation of the nonlinearity in the heterodyne interferometer *Meas. Sci. Technol.* **13** 222–5
- [68] Schmitz T L, Chu D and Houck L I 2006 First-order periodic error correction: validation for constant and non-constant velocities with variable error magnitudes *Meas. Sci. Technol.* **17** 3195–203
- [69] Joo K N, Ellis J D, Spronck J W, van Kan P J and Munnig Schmidt R H 2009 Simple heterodyne laser interferometer with subnanometer periodic errors *Opt. Lett.* **34** 386–8
- [70] Joo K N, Ellis J D, Buice E S, Spronck J W and Schmidt R H 2010 High resolution heterodyne interferometer without detectable periodic nonlinearity *Opt. Express* **18** 1159–65
- [71] Weichert C, Köchert P, König R, Flügge J, Andreas B and Kuetgens U 2012 A heterodyne interferometer with periodic nonlinearities smaller than  $\pm 10\text{ pm}$  *Meas. Sci. Technol.* **23** 2910–6
- [72] Yan L, Chen B, Zhang C, Zhang E and Yang Y 2015 Analysis and verification of the nonlinear error resulting from the misalignment of a polarizing beam splitter in a heterodyne interferometer *Meas. Sci. Technol.* **26** 085006
- [73] Le F S, Salvade Y, Droz N, Mitouassiou R and Favre P 2010 Superheterodyne configuration for two-wavelength interferometry applied to absolute distance measurement *Appl. Opt.* **49** 714–7
- [74] Hsieh H L and Chen W 2016 Heterodyne Wollaston laser encoder for measurement of in-plane displacement *Opt. Express* **24** 8693–707
- [75] Meskers A J, Spronck J W and Munnig Schmidt R H 2014 Validation of separated source frequency delivery for a fiber-coupled heterodyne displacement interferometer *Opt. Lett.* **39** 4603–6
- [76] Wang Y C, Shyu L H and Chang C P 2010 The comparison of environmental effects on Michelson and Fabry–Perot interferometers utilized for the displacement measurement *Sensors* **10** 2577–86
- [77] Gould G, Rabinowitz P, Jacobs S F and Shultz T 1962 Cube-corner Fabry–Perot interferometer *J. Opt. Soc. Am.* **52** 452–3
- [78] Chang C P, Tung P C, Shyu L H, Wang Y C and Manske E 2013 Fabry–Perot displacement interferometer for the measuring range up to 100 mm *Measurement* **46** 4094–9
- [79] Durand M, Lawall J and Wang Y 2011 High-accuracy Fabry–Perot displacement interferometry using fiber lasers *Meas. Sci. Technol.* **22** 094025
- [80] Nowakowski B K, Smith D T and Smith S T 2016 Highly compact fiber Fabry–Perot interferometer: a new instrument design *Rev. Sci. Instrum.* **87** 115102
- [81] Post D 1982 Developments in Moire interferometry *Opt. Eng.* **21** 77–95
- [82] Lu Q, Wang C, Bai J, Wang K, Lian W, Lou S, Jiao X and Yang G 2015 Subnanometer resolution displacement sensor based on a grating interferometric cavity with intensity compensation and phase modulation *Appl. Opt.* **54** 4188–96
- [83] Guo D, Wang M and Hao H 2015 Displacement measurement using a laser feedback grating interferometer *Appl. Opt.* **54** 9320–5
- [84] Kim J, Miskiewicz M N, Serati S and Escuti M J 2015 Nonmechanical laser beam steering based on polymer polarization gratings: design optimization and demonstration *J. Lightwave Technol.* **33** 2068–77
- [85] Hsieh H L and Pan S W 2015 Development of a grating-based interferometer for six-degree-of-freedom displacement and angle measurements *Opt. Express* **23** 2451–65
- [86] Hsieh H L and Pan S W 2013 Three-degree-of-freedom displacement measurement using grating based heterodyne interferometry *Appl. Opt.* **52** 6840–8
- [87] Bonse U and Hart M 1965 An x-ray interferometer *Appl. Phys. Lett.* **6** 155–6
- [88] Hart M 1968 An angstrom ruler *J. Phys. D: Appl. Phys.* **1** 1405
- [89] Massa E, Mana G, Kuetgens U and Ferroglio L 2009 Measurement of the lattice parameter of a silicon crystal *New J. Phys.* **11** 053013
- [90] Yacoot A and Kuetgens U 2012 Sub-atomic dimensional metrology: developments in the control of x-ray interferometers *Meas. Sci. Technol.* **23** 074003
- [91] Basile G *et al* 2000 Combined optical and x-ray interferometry for high-precision dimensional metrology *Proc. R. Soc. A* **456** 701–29
- [92] Donati S, Giuliani G and Merlo S 1995 Laser diode feedback interferometer for measurement of displacements without ambiguity *IEEE J. Quantum Electron.* **31** 113–9
- [93] Palmer A W, Meggitt B T, Grattan K T V and Ning Y 1989 Characteristics of laser diodes for interferometric use *Appl. Opt.* **28** 3657–61
- [94] Gouaux F, Servagent N and Bosch T 1998 Absolute distance measurement with an optical feedback interferometer *Appl. Opt.* **37** 6684–9
- [95] Donati S 2012 Developing self-mixing interferometry for instrumentation and measurements *Laser Photonics Rev.* **6** 393–417
- [96] Shinohara S, Yoshida H, Ikeda H and Nishide K 1992 Compact and high-precision range finder with wide dynamic range and its application *IEEE Trans. Instrum. Meas.* **41** 40–4
- [97] Gagnon E and Rivest J F 1999 Laser range imaging using the self-mixing effect in a laser diode *IEEE Trans. Instrum. Meas.* **48** 693–9
- [98] Kou K, Li X, Li L and Xiang H 2014 Injected current reshaping in distance measurement by laser self-mixing interferometry *Appl. Opt.* **53** 6280–6
- [99] Moench H, Gerlach P and Gronenborn S 2016 VCSEL-based sensors for distance and velocity *Proc. SPIE* **9766** 97660A
- [100] Michalzik R 2012 *VCSELS Fundamentals, Technology and Applications of Vertical-Cavity Surface-Emitting Lasers* (Berlin: Springer)
- [101] Bosch T, Servagent N, Chellali R and Lescure M 1998 Three-dimensional object construction using a self-mixing type

- scanning laser range finder *IEEE Trans. Instrum. Meas.* **47** 1326–9
- [102] Guo D and Wang M 2007 Self-mixing interferometry based on a double-modulation technique for absolute distance measurement *Appl. Opt.* **46** 1486–91
- [103] Polhemus C 1973 Two-wavelength interferometry *Appl. Opt.* **12** 2071–4
- [104] Wyant J C and Cheng Y Y 1984 Two-wavelength phase shifting interferometry *Appl. Opt.* **23** 4539–43
- [105] Dändliker R, Thalmann R and Prongué D 1988 Two-wavelength laser interferometry using superheterodyne detection *Opt. Lett.* **13** 339–41
- [106] Falaggis K, Towers D P and Towers C E 2012 Method of excess fractions with application to absolute distance metrology: wavelength selection and the effects of common error sources *Appl. Opt.* **51** 6471–9
- [107] Cheng Y Y and Wyant J C 1985 Multiple-wavelength phase-shifting interferometry *Appl. Opt.* **24** 804–7
- [108] Meinershagen K, Burgarth V and Abouzeid A 2004 Profilometry with a multi-wavelength diode laser interferometer *Meas. Sci. Technol.* **15** 741–6
- [109] Yang R, Pollinger F, Meinershagen K, Krystek M, Tan J and Bosse H 2015 Absolute distance measurement by dual-comb interferometry with multi-channel digital lock-in phase detection *Meas. Sci. Technol.* **26** 084001
- [110] Kuschmierz R, Czarske J and Fischer A 2014 Multiple wavelength interferometry for distance measurements of moving objects with nanometer uncertainty *Meas. Sci. Technol.* **25** 085202
- [111] Falaggis K, Towers D P and Towers C E 2009 Multiwavelength interferometry: extended range metrology *Opt. Lett.* **34** 950–2
- [112] Sharma S, Eiswirt P and Petter J 2018 Electro optic sensor for high precision absolute distance measurement using multiwavelength interferometry *Opt. Express* **26** 3443–51
- [113] Sa V D B, Persijn S T, Kok G J, Zeitouny M G and Bhattacharya N 2012 Many-wavelength interferometry with thousands of lasers for absolute distance measurement *Phys. Rev. Lett.* **108** 183901
- [114] Kikuta H, Iwata K and Nagata R 1986 Distance measurement by the wavelength shift of laser diode light *Appl. Opt.* **25** 2976–80
- [115] Thiel J, Pfeifer T and Hartmann M 1995 Interferometric measurement of absolute distances of up to 40 m *Measurement* **16** 1–6
- [116] Bechstein K and Fuchs W 1998 Absolute interferometric distance measurements applying a variable synthetic wavelength *J. Opt.* **29** 179–82
- [117] Xiaoli D and Seta K 1999 High-accuracy absolute distance measurement by means of wavelength scanning heterodyne interferometry *Meas. Sci. Technol.* **9** 1031–5
- [118] Cabral A P and Rebordão J M 2007 Accuracy of frequency-sweeping interferometry for absolute distance metrology *Opt. Eng.* **46** 073602
- [119] Kinder T and Salewski K D 2002 Absolute distance interferometer with grating-stabilized tunable diode laser at 633 nm *J. Opt. A: Pure Appl. Opt.* **4** S364–8
- [120] Swinkels B L, Bhattacharya N and Braat J J M 2005 Correcting movement errors in frequency-sweeping interferometry *Opt. Lett.* **30** 2242–4
- [121] Kim S W 2009 Metrology: combs rule *Nat. Photon.* **3** 313–4
- [122] Cundiff S T and Ye J 2003 Femtosecond optical frequency combs *Rev. Mod. Phys.* **75** 325–42
- [123] Wu G, Liao L, Xiong S, Li G, Cai Z and Zhu Z 2018 Synthetic wavelength interferometry of an optical frequency comb for absolute distance measurement *Sci. Rep.* **8** 4362–8
- [124] Minoshima K and Matsumoto H 2000 High-accuracy measurement of 240-m distance in an optical tunnel by use of a compact femtosecond laser *Appl. Opt.* **39** 5512–7
- [125] Jin J 2015 Dimensional metrology using the optical comb of a mode-locked laser *Meas. Sci. Technol.* **27** 022001
- [126] Ye J 2004 Absolute measurement of a long, arbitrary distance to less than an optical fringe *Opt. Lett.* **29** 1153–5
- [127] Cui M, Zeitouny M G, Bhattacharya N, Sa V D B, Urbach H P and Braat J J 2009 High-accuracy long-distance measurements in air with a frequency comb laser *Opt. Lett.* **34** 1982–4
- [128] Wu H, Zhang F, Cao S, Xing S and Qu X 2014 Absolute distance measurement by intensity detection using a mode-locked femtosecond pulse laser *Opt. Express* **22** 10380–97
- [129] Cui M, Schouten R N, Bhattacharya N and Berg S A 2008 Experimental demonstration of distance measurement with a femtosecond frequency comb laser *J. Eur. Opt. Soc. Rapid Publ.* **3** 08003
- [130] Balling P, Kren P, Masika P and Sa V D B 2009 Femtosecond frequency comb based distance measurement in air *Opt. Express* **17** 9300–13
- [131] Zhu J, Cui P, Guo Y, Yang L and Lin J 2015 Pulse-to-pulse alignment based on interference fringes and the second-order temporal coherence function of optical frequency combs for distance measurement *Opt. Express* **23** 13069–81
- [132] Wu G, Takahashi M, Inaba H and Minoshima K 2013 Pulse-to-pulse alignment technique based on synthetic-wavelength interferometry of optical frequency combs for distance measurement *Opt. Lett.* **38** 2140–3
- [133] Shang H T 1981 Chromatic dispersion measurement by white-light interferometry on metre-length single-mode optical fibres *Electron. Lett.* **17** 603–5
- [134] Rao Y J and Jackson D A 1996 Recent progress in fibre optic low-coherence interferometry *Meas. Sci. Technol.* **7** 981–99
- [135] Huang D, Swanson E A, Lin C P, Schuman J S, Stinson W G and Chang W 1991 Optical coherence tomography *Science* **254** 1178–81
- [136] Wang Z B, Shi G H, He Y, Ding Z H and Zhang Y D 2012 Application of optical coherence tomography to distance measurement of optical surface *Opt. Precis. Eng.* **20** 1469–74
- [137] Danielson B L and Boisrobert C Y 1991 Absolute optical ranging using low coherence interferometry *Appl. Opt.* **30** 2975
- [138] PavláCek P and Häusler G 2005 White-light interferometer with dispersion: an accurate fiber-optic sensor for the measurement of distance *Appl. Opt.* **44** 2978–83
- [139] Majumdar A and Huang H 2008 Development of an in-fiber white-light interferometric distance sensor for absolute measurement of arbitrary small distances *Appl. Opt.* **47** 2821–8
- [140] Ullmann V, Emam S and Manske E 2015 White-light interferometers with polarizing optics for length measurements with an applicable zero-point detection *Meas. Sci. Technol.* **26** 084010
- [141] Koch A and Ulrich R 1990 Fiber-optic displacement sensor with 0.02  $\mu\text{m}$  resolution by white-light interferometry *Sens. Actuators A* **25** 201–7
- [142] Winarno A, Masuda S, Takahashi S, Matsumoto H and Takamasu K 2018 Noncontact method of point-to-point absolute distance measurement using tandem low-coherence interferometry *Meas. Sci. Technol.* **29** 025006
- [143] Winarno A, Takahashi S, Hirai A, Takamasu K and Matsumoto H 2012 Absolute measurement of gauge block without wringing using tandem low-coherence interferometry *Meas. Sci. Technol.* **23** 125001

- [144] Carre P 1966 Installation et utilisation du comparateur photoélectrique et interferentiel du Bureau International des Poids et Mesures *Metrologia* **2** 13–23
- [145] Bruning J H, Herriott D R, Gallagher J E, Rosenfeld D P, White A D and Brangaccio D J 1976 Digital wavefront measuring interferometer for testing optical surfaces and lenses *Appl. Opt.* **13** 2693–703
- [146] Schreiber H and Bruning J H 2006 Phase shifting interferometry *Optical Shop Testing* ed D Malacara (Hoboken, NJ: Wiley) (<https://doi.org/10.1002/9780470135976.ch14>)
- [147] Medecki H, Tejnil E, Goldberg K A and Bokor J 1996 Phase-shifting point diffraction interferometer *Opt. Lett.* **21** 1526–8
- [148] Huang P S and Zhang S 2006 Fast three-step phase-shifting algorithm *Appl. Opt.* **45** 5086–91
- [149] Schmit J and Creath K 1995 Extended averaging technique for derivation of error-compensating algorithms in phase-shifting interferometry *Appl. Opt.* **34** 3610–9
- [150] Hutter T, Elliott S R and Ruschin S 2013 Dynamic range enhancement and phase-ambiguity elimination in wavelength-interrogated interferometric sensor *Sens. Actuators B* **178** 593–7
- [151] Grassani D, Galli M and Bajoni D 2014 Active stabilization of a Michelson interferometer at an arbitrary phase with subnanometer resolution *Opt. Lett.* **39** 2530–3
- [152] Lee B S and Strand T C 1990 Profilometry with a coherence scanning microscope *Appl. Opt.* **29** 3784–8
- [153] Warnasooriya N and Kim M K 2007 LED-based multi-wavelength phase imaging interference microscopy *Opt. Express* **15** 9239–47
- [154] Fei L, Lu X, Wang H, Zhang W, Tian J and Zhong L 2014 Single-wavelength phase retrieval method from simultaneous multi-wavelength in-line phase-shifting interferograms *Opt. Express* **22** 30910–23
- [155] Takahashi T, Ishii Y and Onodera R 2014 Phase-shifting interferometric profilometry with a wavelength-tunable diode source *Opt. Rev.* **21** 410–4
- [156] Sandoz P, Devillers R and Plata A 1997 Unambiguous profilometry by fringe-order identification in white-light phase-shifting interferometry *J. Mod. Opt.* **44** 519–34
- [157] Chen L C, Yeh S L, Tapilouw A M and Chang J C 2010 3-D surface profilometry using simultaneous phase-shifting interferometry *Opt. Commun.* **283** 3376–82
- [158] Goldberg K A and Bokor J 2001 Fourier-transform method of phase-shift determination *Appl. Opt.* **40** 2886–94
- [159] Wang Z and Han B 2004 Advanced iterative algorithm for phase extraction of randomly phase-shifted interferograms *Opt. Lett.* **29** 1671–3
- [160] Gao P, Yao B, Lindlein N, Mantel K, Harder I and Geist E 2009 Phase-shift extraction for generalized phase-shifting interferometry *Opt. Lett.* **34** 3553–5
- [161] Vargas J, Quiroga J A and Belenguer T 2011 Analysis of the principal component algorithm in phase-shifting interferometry *Opt. Lett.* **36** 2215–7
- [162] Menesesfabian C and Laracortes F A 2015 Phase retrieval by Euclidean distance in self-calibrating generalized phase-shifting interferometry of three steps *Opt. Express* **23** 13589–604
- [163] Shou J, Zhong L, Zhou Y, Tian J and Lu X 2017 Phase shifts extraction based on time-domain orthogonal character of phase-shifting interferograms *Opt. Commun.* **382** 444–9
- [164] Northmorris M B, Millerd J E, Brock N J and Hayes J B 2004 Phase-shifting multiwavelength dynamic interferometer *Proc. SPIE* **5531** 64–75
- [165] Dubois A, Vabre L and Boccara A C 2001 Sinusoidally phase-modulated interference microscope for high-speed high-resolution topographic imagery *Opt. Lett.* **26** 1873–5
- [166] Schmit J, Reed J, Novak E and Gimzewski J K 2008 Performance advances in interferometric optical profilers for imaging and testing *J. Opt. A: Pure Appl. Opt.* **10** 064001
- [167] Schwarz C J, Kuznetsova Y and Brueck S R J 2003 Imaging interferometric microscopy *Opt. Lett.* **28** 1424–6
- [168] Wyant J C, Koliopoulos C L, Bhushan B and George O E 1984 An optical profilometer for surface characterization of magnetic media *ASLE Trans.* **27** 101–13
- [169] Safrani A and Abdulhalim I 2014 Real-time phase shift interference microscopy *Opt. Lett.* **39** 5220–3
- [170] Kinnstaetter K, Lohmann A W, Schwider J and Streibl N 1988 Accuracy of phase shifting interferometry *Appl. Opt.* **27** 5082–9
- [171] Schmit J 2008 Iterative algorithm for phase shifting interferometry with finite bandwidth illumination *Proc. SPIE* **7063** 70630L
- [172] Levin G G, Vishnyakov G N, Moiseev N N and Minaev V L 2013 The lateral resolution of an interference microscope *Meas. Tech.* **56** 486–91
- [173] Arvidson R S, Fischer C, Sawyer D S, Scott G D, Natelson D and Luttge A 2014 Lateral resolution enhancement of vertical scanning interferometry by sub-pixel sampling *Microsc. Microanal.* **20** 90–8
- [174] De Groot P J and Biegen J F 2016 Interference microscope objectives for wide-field areal surface topography measurements *Opt. Eng.* **55** 074110
- [175] Creath K 1989 Calibration of numerical aperture effects in interferometric microscope objectives *Appl. Opt.* **28** 3333–8
- [176] Dubois A 2004 Effects of phase change on reflection in phase-measuring interference microscopy *Appl. Opt.* **43** 1503–7
- [177] Balasubramanian N 1983 Optical system for surface topography measurement *US Patent Specification* 4340306A
- [178] Schmit J and Olszak A 2002 High-precision shape measurement by white-light interferometry with real-time scanner error correction *Appl. Opt.* **41** 5943–50
- [179] Lehmann P, Tereshchenko S and Xie W 2016 Fundamental aspects of resolution and precision in vertical scanning white-light interferometry *Surf. Topogr. Metrol. Prop.* **4** 024004
- [180] Tian A 2008 Study on key algorithm for scanning white-light interferometry *Proc. SPIE* **7155** 71552N
- [181] Lei Z, Liu X, Chen L, Lu W and Chang S 2016 A novel surface recovery algorithm in white light interferometry *Measurement* **80** 1–11
- [182] De Groot P, De Lega X C, Kramer J and Turzhitsky M 2002 Determination of fringe order in white-light interference microscopy *Appl. Opt.* **41** 4571–8
- [183] Chen D 2009 High-definition vertical-scan interferometry *US Patent Specification* 7605925
- [184] Ma S, Quan C, Zhu R, Tay C J and Chen L 2011 Surface profile measurement in white-light scanning interferometry using a three-chip color CCD *Appl. Opt.* **50** 2246–54
- [185] Ma S, Quan C, Zhu R, Tay C J, Chen L and Gao Z 2011 Micro-profile measurement based on windowed Fourier transform in white-light scanning interferometry *Opt. Commun.* **284** 2488–93
- [186] Tan J, Wang C, Wang Y, Wang W, Liu J, Leach R and Hao L 2014 Long working distance microscope with a low obscuration aspherical Schwarzschild objective *Opt. Lett.* **39** 6699–702
- [187] Lei Z, Liu X, Zhao L, Chen L, Li Q, Yuan T and Lu W 2016 A novel 3D stitching method for WLI based large range surface topography measurement *Opt. Commun.* **359** 435–47

- [188] Pförtner A and Schwider J 2003 Red-green-blue interferometer for the metrology of discontinuous structures *Appl. Opt.* **42** 667–73
- [189] Kumar U P, Haifeng W, Mohan N K and Kothiyal M P 2012 White light interferometry for surface profiling with a colour CCD *Opt. Lasers Eng.* **50** 1084–8
- [190] Upputuri P K, Gong L, Wang H, Pramanik M, Nandigana K M and Kothiyal M P 2014 Measurement of large discontinuities using single white light interferogram *Opt. Express* **22** 27373–80
- [191] Srivastava V, Inam M, Kumar R and Mehta D S 2017 Single shot white light interference microscopy for 3D surface profilometry using single chip color camera *J. Opt. Soc. Korea* **20** 784–93
- [192] Qi W 2015 Random errors for the measurement of central positions in white-light interferometry with the least-squares method *J. Opt. Soc. Am. A* **32** 1536–43
- [193] Tereschenko S, Lehmann P, Gollor P and Kuehnhold P 2015 Robust vertical scanning white-light interferometry in close-to-machine applications *Proc. SPIE* **9525** 95250Q
- [194] Gabor D 1948 A new microscopic principle *Nature* **161** 777–8
- [195] Yamaguchi I and Zhang T 2009 Phase-shifting digital holography *Opt. Lett.* **22** 1268
- [196] Wagner C, Osten W and Seebacher S 2000 Direct shape measurement by digital wavefront reconstruction and multi-wavelength contouring *Opt. Eng.* **39** 79–85
- [197] Aleksoff C C 2006 Multi-wavelength digital holographic metrology *Proc. SPIE* **6311** 63111D
- [198] Dong J, Jiang C and Jia S 2016 Digital holographic metrology based on multi-angle interferometry *Opt. Lett.* **41** 4301–4
- [199] Francis D, Tatam R P and Groves R M 2010 Shearography technology and applications: a review *Meas. Sci. Technol.* **21** 102001
- [200] Wyant J C 1973 Double frequency grating lateral shear interferometer *Appl. Opt.* **12** 2057–60
- [201] Nomura T, Kamiya K, Miyashiro H, Okuda S, Tashiro H and Yoshikawa K 1998 Shape measurements of mirror surfaces with a lateral-shearing interferometer during machine running *Precis. Eng.* **22** 185–9
- [202] Mehta D S, Dubey S K, Hossain M M and Shakher C 2005 Simple multifrequency and phase-shifting fringe-projection system based on two-wavelength lateral shearing interferometry for three-dimensional profilometry *Appl. Opt.* **44** 7515–21
- [203] Ghim Y S, Rhee H G, Davies A, Yang H S and Lee Y W 2014 3D surface mapping of freeform optics using wavelength scanning lateral shearing interferometry *Opt. Express* **22** 5098–105
- [204] Sommargren G E 1981 Optical heterodyne profilometry *Appl. Opt.* **20** 610–8
- [205] Sommargren G E 1981 An optical measurement of surface profile *Precis. Eng.* **3** 131–6
- [206] Badami V and De Groot P 2013 Displacement measuring interferometry *Meas. Sci. Technol.* **4** 157–238
- [207] Zhao H, Liang R, Li D and Cao M 2001 Practical common-path heterodyne surface profiling interferometer with automatic focusing *Opt. Laser Technol.* **33** 259–65
- [208] Kokuyama W, Nozato H, Ohta A and Hattori K 2016 Simple digital phase-measuring algorithm for low-noise heterodyne interferometry *Meas. Sci. Technol.* **27** 085001
- [209] Somervell A R D, Williams M E K and Barnes T H 2004 Direct measurement of fringe amplitude and phase using a heterodyne interferometer operating in broadband light *Opt. Commun.* **229** 59–64
- [210] Lin Y, Schill J and Wang R W 1994 Instrumental noise effect in an optical heterodyne profiler *Appl. Opt.* **33** 5005–10
- [211] Chiu M H, Chen W C and Tan C T 2015 Small displacement measurements based on an angular-deviation amplifier and interferometric phase detection *Appl. Opt.* **54** 2885–90
- [212] Park S J, Eom J, Kim Y H, Lee C S and Lee B H 2014 Noncontact photoacoustic imaging based on all-fiber heterodyne interferometer *Opt. Lett.* **39** 4903–6
- [213] Baltazar R, Solano C and Martínez-Ponce G 2002 Optical heterodyne profilometer to scan irregularities in reflective objects *Opt. Commun.* **204** 33–43
- [214] Dash J N, Jha R, Villatoro J and Dass S 2015 Nano-displacement sensor based on photonic crystal fiber modal interferometer *Opt. Lett.* **40** 467–70
- [215] Balboa I, Ford H D and Tatam R P 2006 Low-coherence optical fibre speckle interferometry *Meas. Sci. Technol.* **17** 605–16
- [216] Xia W and Chen X 2016 Recent developments in fiber-based optical frequency comb and its applications *Meas. Sci. Technol.* **27** 041001
- [217] Lin D, Jiang X, Xie F, Zhang W, Zhang L and Bennion I 2004 High stability multiplexed fiber interferometer and its application on absolute displacement measurement and on-line surface metrology *Opt. Express* **12** 5729–34
- [218] Zheng J 2007 Triple-sensor multiplexed frequency-modulated continuous-wave interferometric fiber-optic displacement sensor *Appl. Opt.* **46** 2189–96
- [219] Kissinger T, Charrett T O H and Tatam R P 2015 Range-resolved interferometric signal processing using sinusoidal optical frequency modulation *Opt. Express* **23** 9415–31
- [220] Kissinger T, Charrett T O H, James S W, Adams A, Twin A and Tatam R P 2015 Simultaneous laser vibrometry on multiple surfaces with a single beam system using range-resolved interferometry *Proc. SPIE* **9525** 952520
- [221] Martin H and Jiang X 2010 Rapid phase-shifting fiber interferometer with optical stylus *Opt. Lett.* **35** 655–7
- [222] Jiang X, Wang K and Martin H 2006 Near common-path optical fiber interferometer for potentially fast on-line microscale-nanoscale surface measurement *Opt. Lett.* **31** 3603–5
- [223] Jusko O, Neugebauer M, Reimann H, Drabarek P, Fleischer M and Gnausch T 2009 Form measurements by optical and tactile scanning *Proc. SPIE* **7133** 71333A
- [224] Schwider J and Zhou L 1994 Dispersive interferometric profilometer *Opt. Lett.* **19** 995–7
- [225] Debnath S K, Kim S W, Kothiyal M P and Hariharan P 2010 Spectrally resolved phase-shifting interference microscopy: technique based on optical coherence tomography for profiling a transparent film on a patterned substrate *Appl. Opt.* **49** 6624–9
- [226] Groot P D 1991 Three-color laser-diode interferometer *Appl. Opt.* **30** 3612–6
- [227] Am Weg C, Berger G, May T, Nicolaus R and Petter J 2014 Method and device for measuring surfaces in a highly precise manner *US Patent Specification* 8736850 B2
- [228] Hahn R, Krauter J, Koerner K, Gronle M and Osten W 2017 Single-shot low coherence pointwise measuring interferometer with potential for in-line inspection *Meas. Sci. Technol.* **28** 025009
- [229] Jiang X 2012 Precision surface measurement *Phil. Trans. R Soc. A* **370** 4089–114
- [230] Palmer C A and Loewen E G 2005 *Diffraction Grating Handbook* (New York: Newport Corporation)
- [231] Cole D B, Sorace-Agaskar C, Moresco M, Leake G, Coolbaugh D and Watts M R 2015 Integrated heterodyne interferometer with on-chip modulators and detectors *Opt. Lett.* **40** 3097–100
- [232] Kumar P, Martin H and Jiang X 2016 Towards the development of a hybrid-integrated chip interferometer for online surface profile measurements *Rev. Sci. Instrum.* **87** 065103

- [233] Tabibazar M 1997 Modern trends in microstructures and integrated optics for communication, sensing, and actuation *Opt. Eng.* **36** 1307–18
- [234] Yang S, Jiang X, Maxwell G and Wang K 2008 An integrated optical coupler used in a fiber interferometry system for on-line surface measurements *Opt. Commun.* **281** 1099–107
- [235] Yang S, Jiang X, Maxwell G, Wyatt R and Rogers D 2010 A chip tunable laser developed for on-line micro-nano scale surface measurements *Meas. Sci. Technol.* **21** 105901
- [236] Calatroni J, Guerrero A L, Sáinz C and Escalona R 1996 Spectrally-resolved white-light interferometry as a profilometry tool *Opt. Laser Technol.* **28** 485–9
- [237] Sandoz P, Tribillon G and Perrin H 1996 High-resolution profilometry by using phase calculation algorithms for spectroscopic analysis of white-light interferograms *Opt. Acta Int. J. Opt.* **43** 701–8
- [238] Debnath S K and Kothiyal M P 2006 Improved optical profiling using the spectral phase in spectrally resolved white-light interferometry *Appl. Opt.* **45** 6965–72
- [239] Debnath S K and Kothiyal M P 2006 Analysis of spectrally resolved white light interferometry by Hilbert transform method *Proc. SPIE* **6292** 62920P
- [240] Hlubina P, Luňáček J, Ciprian D and Chlebus R 2008 Windowed fourier transform applied in the wavelength domain to process the spectral interference signals *Opt. Commun.* **281** 2349–54
- [241] Bethge J, Grebing C and Steinmeyer G 2007 A fast Gabor wavelet transform for high-precision phase retrieval in spectral interferometry *Opt. Express* **15** 14313–21
- [242] Debnath S K, Kothiyal M P and Kim S W 2009 Evaluation of spectral phase in spectrally resolved white-light interferometry: comparative study of single-frame techniques *Opt. Lasers Eng.* **47** 1125–30
- [243] Fleig J, Dumas P, Murphy P E and Forbes G W 2003 An automated subaperture stitching interferometer workstation for spherical and spherical surfaces *Proc. SPIE* **5188**
- [244] Millerd J E, Brock N J, Hayes J B, Northmorris M B, Novak M and Wyant J C 2004 Pixelated phase-mask dynamic interferometer *Proc. SPIE* **5531** 304–14
- [245] Kuchel M F 2009 Interferometric measurement of rotationally symmetric aspheric surfaces *Proc. SPIE* **7389** 738916
- [246] Garbusi E, Pruss C and Osten W 2008 Interferometer for precise and flexible asphere testing *Opt. Lett.* **33** 2973–5
- [247] Pruss C, Baer G B, Schindler J and Osten W 2017 Measuring aspheres quickly: tilted wave interferometry *Opt. Eng.* **56** 111713
- [248] Weckenmann A, Jiang X, Sommer K D, Neuschafer-Rube U, Seewig J, Shaw L and Estler T 2009 Multisensor data fusion in dimensional metrology *CIRP Ann.-Manuf. Technol.* **58** 701–21
- [249] Durrant-Whyte H F 1988 Sensor models and multisensor integration *Int. J. Robot. Res.* **7** 97–113
- [250] Michel F R, Piron P, Renotte Y L and Habraken S 2013 Combining shearography and interferometric fringe projection in a single device for complete control of industrial applications *Opt. Eng.* **52** 084102
- [251] Kujawinska M 2002 Modern optical measurement station for micro-materials and micro-elements studies *Sens. Actuators A* **99** 144–53
- [252] Gastinger K, Haugolt K H, Kujawinska M, Jozwik M, Schaeffel C and Beer S 2009 Optical, mechanical, and electro-optical design of an interferometric test station for massive parallel inspection of MEMS and MOEMS *Proc. SPIE* **7389** 58–60
- [253] Jager G, Hausotte T, Manske E, Buchner H J, Mastyllo R, Dorozhovets N and Hoffmann N 2010 Nanomeasuring and nanopositioning engineering *Measurement* **43** 1099–105
- [254] Gronle M and Osten W 2016 View and sensor planning for multi-sensor surface inspection *Surf. Topogr. Metrol. Prop.* **4** 024009
- [255] Guo T, Wang S, Dorantesgonzalez D J, Chen J, Fu X and Hu X 2011 Development of a hybrid atomic force microscopic measurement system combined with white light scanning interferometry *Sensors* **12** 175–88
- [256] Manske E, Hausotte T, Mastyllo R, Machleidt T, Franke K H and Jager G 2007 New applications of the nanopositioning and nanomeasuring machine by using advanced tactile and non-tactile probes *Meas. Sci. Technol.* **18** 520–7
- [257] Vorbringer-Dorozhovets N, Goj B, Machleidt T, Franke K H, Hoffmann M and Manske E 2014 Multifunctional nanoanalytics and long-range scanning probe microscope using a nanopositioning and nanomeasuring machine *Meas. Sci. Technol.* **25** 044006
- [258] Park J, Lee M Y and Lee D Y 2009 A nano-metrology system with a two-dimensional combined optical and x-ray interferometer and an atomic force microscope *Microsyst. Technol.* **15** 1879–84
- [259] Jobin M, Passeraub P and Foschia R 2006 Nanometrology for MEMS: combination of optical interference, atomic force microscopy, and nanoindenter-based actuator *Proc. SPIE* **6188** 61880T
- [260] Leach R K, Claverley J, Giusca C, Jones C W, Nimishakavi L, Sun W, Tedaldi M and Yacoot A 2012 Advances in engineering nanometrology at the National Physical Laboratory *Meas. Sci. Technol.* **23** 74002–10
- [261] Manske E, Jager G, Hausotte T and Fusharpl R 2012 Recent developments and challenges of nanopositioning and nanomeasuring technology *Meas. Sci. Technol.* **23** 074001
- [262] Dai G, Zhu F and Fluegge J 2015 High-speed metrological large range AFM *Meas. Sci. Technol.* **26** 095402
- [263] Tasic T and Acko B 2011 Integration of a laser interferometer and a CMM into a measurement system for measuring internal dimensions *Measurement* **44** 426–33
- [264] Ettemeyer A 2012 New three-dimensional fiber probe for multisensor coordinate measurement *Opt. Eng.* **51** 081502
- [265] Albertazzi A G, Hofmann A C, Fantin A V and Santos J M C 2008 Photogrammetric endoscope for measurement of inner cylindrical surfaces using fringe projection *Appl. Opt.* **47** 3868–76
- [266] Buckner B, Heeg B, Jenkins T and Trolinger J 2014 Microscopic contouring with low coherence interferometry endoscopy *Proc. SPIE* **9204** 920402
- [267] Gao Y, Wu S, Zhu L and Yang L 2015 Investigation of hidden diffuse surfaces using phase-shifting endoscopic digital speckle pattern interferometry *Proc. SPIE* **9446** 94463J
- [268] Matthias S, Kastner M and Reithmeier E 2015 Evaluation of system models for an endoscopic fringe projection system *Measurement* **73** 239–46
- [269] Li C, Ning T, Zhang C, Li J, Zhang C, Wen X, Lin H and Pei L 2016 All-fiber multipath Mach-Zehnder interferometer based on a four-core fiber for sensing applications *Sens. Actuators A* **248** 148–54